



Article

Combined Metabolome and Transcriptome Analysis Elucidates Sugar Accumulation in Wucai (*Brassica campestris* L.)

Chenggang Wang ^{1,2,†} , Jiajie Zhou ^{1,2,†}, Shengnan Zhang ^{1,2}, Xun Gao ^{1,2}, Yitao Yang ^{1,2}, Jinfeng Hou ^{1,2}, Guohu Chen ^{1,2}, Xiaoyan Tang ^{1,2}, Jianqiang Wu ^{1,2} and Lingyun Yuan ^{1,2,*}

¹ College of Horticulture, Vegetable Genetics and Breeding Laboratory, Anhui Agricultural University, 130 West Changjiang Road, Hefei 230036, China

² Provincial Engineering Laboratory for Horticultural Crop Breeding of Anhui, 130 West of Changjiang Road, Hefei 230036, China

* Correspondence: yuanlingyun@ahau.edu.cn; Tel./Fax: +86-0551-65786212

† These authors contributed equally to this work.

Abstract: Wucai (*Brassica campestris* L.) is a leafy vegetable that originated in China, its soluble sugars accumulate significantly to improve taste quality during maturation, and it is widely accepted by consumers. In this study, we investigated the soluble sugar content at different developmental stages. Two periods including 34 days after planting (DAP) and 46 DAP, which represent the period prior to and after sugar accumulation, respectively, were selected for metabolomic and transcriptomic profiling. Differentially accumulated metabolites (DAMs) were mainly enriched in the pentose phosphate pathway, galactose metabolism, glycolysis/gluconeogenesis, starch and sucrose metabolism, and fructose and mannose metabolism. By orthogonal projection to latent structures-discriminant s-plot (OPLS-DA S-plot) and MetaboAnalyst analyses, D-galactose and β -D-glucose were identified as the major components of sugar accumulation in wucai. Combined with the transcriptome, the pathway of sugar accumulation and the interact network between 26 DEGs and the two sugars were mapped. *CWINV4*, *CEL1*, *BGLU16*, and *BraA03g023380.3C* had positive correlations with the accumulation of sugar accumulation in wucai. The lower expression of *BraA06g003260.3C*, *BraA08g002960.3C*, *BraA05g019040.3C*, and *BraA05g027230.3C* promoted sugar accumulation during the ripening of wucai. These findings provide insights into the mechanisms underlying sugar accumulation during commodity maturity, providing a basis for the breeding of sugar-rich wucai cultivars.

Keywords: wucai (*Brassica campestris* L.); D-galactose; β -D-glucose; sugar accumulation pathway; interact network



Citation: Wang, C.; Zhou, J.; Zhang, S.; Gao, X.; Yang, Y.; Hou, J.; Chen, G.; Tang, X.; Wu, J.; Yuan, L. Combined Metabolome and Transcriptome Analysis Elucidates Sugar Accumulation in Wucai (*Brassica campestris* L.). *Int. J. Mol. Sci.* **2023**, *24*, 4816. <https://doi.org/10.3390/ijms24054816>

Academic Editor: Soulaïman Sakr

Received: 1 December 2022

Revised: 18 February 2023

Accepted: 23 February 2023

Published: 2 March 2023



Copyright: © 2023 by the authors. Licensee MDPI, Basel, Switzerland. This article is an open access article distributed under the terms and conditions of the Creative Commons Attribution (CC BY) license (<https://creativecommons.org/licenses/by/4.0/>).

1. Introduction

Wucai (*Brassica campestris* L. ssp. *chinensis* var. *rosularis* Tsen), a subspecies of non-heading Chinese cabbage, is widely grown in the Yangtze-Huai River Basin [1]. Wucai is rich in vitamin C, vitamin B1, and carotene, resulting in it being referred to as a “vitamin vegetable” [2]. Wucai leaves become sweet after undergoing autumn and winter growth, satisfying consumer preference due to their nutritional value and taste [3].

The sweetness of vegetables and fruit depends not only on the total amount of sugar but also on the sugar composition [4]. Sweetness is mainly conferred by sucrose, glucose, and fructose, which contribute differently to the sweetness of vegetables and fruit [4]. In Chinese cabbage, the leafy head is the storage organ and the internal midrib (IM) is the main tissue of sugar accumulation, which possesses the highest content of soluble sugar at harvest [5]. Fructose is the major sugar that accumulates in the internal tissues of Chinese cabbage, followed by glucose [5]. Differences in the sweetness of *Cucurbita moschata* were attributed to the content and composition ratio of sucrose [4,6]. As fructose tastes sweeter than sucrose and glucose, sucrose metabolism and the ratio of fructose/glucose were

promoted in tomato fruits in order to improve the flavor quality [7,8]. The accumulation pattern and concentration of sugar vary with species and are regulated by fruit development [9]. Glucose is the main soluble sugar in mature pitaya fruit, whereas in ripened apricot fruits, glucose and sucrose are the major sugars [10,11]. The contents of sucrose, glucose, and fructose are high in harvested watermelon and mango fruit [12,13]. In melon fruit and sugarcane, sucrose was found to increase steadily with fruit development [14,15].

Sugar accumulation comes mainly from the transport of photosynthetic products, with sucrose being the form of transport in most plants, and a number of key enzymes can be involved in regulating sugar metabolism and, thus, the composition and content of sugars [16]. Sucrose phosphate synthase (SPS), one of the key enzymes in plant sucrose synthesis, catalyzes the production of sucrose as an irreversible reaction and is the rate-limiting enzyme for the synthesis of sucrose [17]. SPS activity is positively correlated with sucrose accumulation [18]. Transcript levels of *SPS* increased with sucrose accumulation during ripening in watermelon and banana [19,20]. In addition, the expression pattern of *SPS* in pineapple and potato all showed that its expression was related to sucrose metabolism [21,22]. Sucrose synthase (SUS) catalyzes both the breakdown of sucrose to UDP glucose and the synthesis of sucrose [17]. SUS is also one of the key enzymes for the entry of sucrose into various metabolic pathways, regulating the ability of the crop to metabolize sucrose and the amount of sucrose input [23]. During the development of apple fruit, with the accumulation of sucrose, the expression of *MdSUSY2*, *MdSUSY3*, and *MdSUSY4* decreased obviously, indicating that SUS mainly played a major role in the decomposition of apple sucrose [24]. The expression of *CitSus5* was increasing while that of *CitSus6* was gradually decreasing during fruit development in citrus, suggesting that SUS was involved in reversible reactions in citrus, possibly both synthesizing and breaking down sucrose [25]. Invertase (INV), also called sucrose, can hydrolyze sucrose into glucose and fructose. According to the site where the enzyme is present on the cell, INV mainly consists of cell wall invertase (CWINV), vesicle invertase (VINV), and cytoplasmic invertase (CINV) [26]. Based on the optimum *PH* of the enzyme, CWINV and VINV can be classified as acid invertase (AI), while CINV is a neutral invertase (NI) [26]. Numerous studies showed that there is a significant negative correlation between the activity of INV and sucrose accumulation in fruits [12,22,26,27]. In tomato fruits, CWINV and VINV are encoded by *LIN* and *VI*, respectively. *LIN5*, *LIN7*, *LIN8*, *LIN9*, and *VI* were upregulated by silencing *SWEET7* (Sugars Will Eventually be Exported Transporters) and *SWEET14* to increase CWINV and VINV activity [28]. It can be seen that the upregulation of CWINV and VINV increases the activities of AI, thereby promoting the hydrolysis of sucrose. CWINV is typically considered as a sink-specific enzyme, and its activity is usually low in source leaves [29]. However, both *MdCWINVs* (*MdCWINV2* and *MdCWINV3*) identified in apple had lower expression levels in the fruit than in the leaves, and the transcript levels of *MdCWINV2* and *MdCWINV3* declined dramatically during maturation [24]. Hexokinase (HK) could catalyze the phosphorylation of hexose, which could catalyze the conversion of glucose into glucose-6-phosphate (glucose-6P), and then enter the glycolytic pathway [30]. Overexpression of the *HK* was able to cause a significant reduction in the sugar content of plants [31].

Besides INV, SPS, and SUS, another enzyme related to sugar accumulation and metabolism in watermelon fruits is α -galactosidase [32]. Stachyose and raffinose are the main transportation forms of photosynthetic products in *Cucurbitaceae* plants, which can be decomposed by α -galactosidase to produce sucrose and galactose [33,34]. Cellulase (CL) is an important enzyme complex, mainly consisting of endoglucanase (EG), exoglucanase (CBH), and β -glucosidase (BGL), which hydrolyze cellulose to form glucose [35–37]. In previous studies, cellulose was considered to be related to the softening of crops during development [38,39]. Nevertheless, in biomass utilization, CL is employed to hydrolyze cellulose in multiple steps to generate glucose [40]. In studies of sugar accumulation in Chinese cabbage that is more closely related to wucai, it was noted that *BraA01gHT4* and *BraA03gHT7* were positively correlated with the soluble sugar content (mainly fructose

and glucose) of the inner lobe, while *BraA03gFRK1*, *BraA09gFRK3*, *BraA06gSPS2*, and *BraA03gHT3* were negatively correlated with sugar content [41]. Furthermore, the high expression of *SUS1* was considered to promote the accumulation of fructose and glucose in leaf balls of Chinese cabbage [42]. Sweetness is a typical indicator and characteristic of maturation in wucaï. In recent years, metabolomics (including liquid chromatography-tandem mass spectrometry (LC-MS/MS) and gas chromatography-tandem mass spectrometry (GC-MS/MS)) and transcriptomics (RNA sequencing (RNA-Seq)) have been successfully applied to reveal the mechanism of sugar accumulation in ripening fruits, such as Chinese cabbage, ponkan, and kiwifruit [41,43,44]. However, there are no studies that have reported on sugar accumulation during wucaï maturation.

A biomarker is a characteristic biochemical index, which can be objectively measured to provide information about the biological process of the organism [45]. Metabonomics pays attention to the changes in small-molecule metabolites in organisms, which provides the possibility for identifying objective biomarkers. Scholars established and analyzed the OPLS-DA model or OPLS-DA-Plot map, and then potential biomarkers could be found in the project based on variable importance in the projection (VIP) score > 1 [46,47]. ROC (receiver operating characteristic curve) and AUC (area under ROC curve) diagnostics were performed using the online software MetaboAnalyst to identify potential biomarkers [46,47]. Combined analyses of the transcriptome and metabolome by LC-MS/MS and GC-MS/MS were conducted herein to investigate the molecular mechanism of sugar transformation in wucaï during the maturation process, and the DAMs and related genes were identified. This is the first report on sugar biomarkers and the mechanisms of sugar accumulation with the maturity process of wucaï. The results provide a valuable basis and reference for commercial applications and breeding programs for wucaï.

2. Results

2.1. Changes in Sugar Content in the Wucai Leaves

A growth chamber was used for simulating the growth environment of wucaï. To investigate the changes in soluble sugar content in wucaï leaves during the growth period, we determined the soluble sugar content at nine sampling periods (Supplementary Figure S1). The results showed that the soluble sugar increased gradually with the growth of wucaï from 34 DAP and peaked at 46 DAP (Figure 1A). The time points of 34 DAP and 46 DAP were selected for the determination of D-galactose, glucose, fructose, and sucrose. It was found that the contents of D-galactose, glucose, and fructose increased significantly during the wucaï maturation process (Figure 1B,C). The contents of D-galactose, fructose, and sucrose at 46 DAP were 1.40-, 1.16-, and 1.39-fold higher than those at 34 DAP, respectively (Figure 1B,D,E). There were significant differences in glucose between the two periods, reaching 3.58-fold (Figure 1C). Interestingly, at 46 DAP, the ratio of glucose/soluble sugar increased to 5.75% from 2.49% at 34 DAP, compared to D-galactose (Figure 1F,G). Therefore, we considered that these sugars, especially glucose, play vital roles in sugar transformation in wucaï. According to the sugar change trend, 34 DAP and 46 DAP were selected as the two periods for further study.

2.2. DAM Analysis in Wucai Leaves

To further understand the changes in metabolites in the wucaï leaves during sugar transformation, the metabolites at 34 DAP and 46 DAP were detected by LC-MS/MS and GC-MS/MS. The PCA of the metabolomic profiles of the 12 samples showed that the first principal component explained 46% (LC-MS/MS) and 47.2% (GC-MS/MS) of the total variance and distinguished the samples based on the two periods (34 DAP and 46 DAP) (Supplementary Figure S2). A total of 650 and 111 DAMs were identified with $p < 0.05$ and $VIP > 1$ from the LC-MS/MS and GC-MS/MS analysis, respectively (Supplementary Figure S3). In the LC-MS/MS analysis, compared to 34 DAP, a total of 385 DAMs were upregulated (fold change, $\log_2(FC) > 0$) and 265 DAMs were downregulated ($\log_2(FC) < 0$) at 46 DAP (Supplementary Figure S3A). The proportion of organooxy-

gen compounds/total DAMs was 12.923%, which was the maximum in any class category (Supplementary Table S1). The organooxygen compounds mainly included 66 carbohydrates and carbohydrate conjugates, nine phenols and polyols, six carbonyl compounds, and three ethers (Figure 2A). The proportion of carbohydrates and carbohydrate conjugates/total DEMs accounted for 10.15%, which was significantly higher than those of the other metabolites according to the sub-class category (Supplementary Table S1). The metabolomic analysis showed that the DAMs were mainly enriched in carbohydrates and carbohydrate conjugates. There were 35 upregulated and 31 downregulated DAMs (Figure 2B). The GC-MS/MS analysis showed that there were 43 upregulated and 68 downregulated DAMs at 46 DAP compared to at 34 DAP (Supplementary Figure S3B). Only 13 DAMs (seven upregulated and six downregulated) were classified as carbohydrates and carbohydrate conjugates (Supplementary Table S2 and Figure 2C).

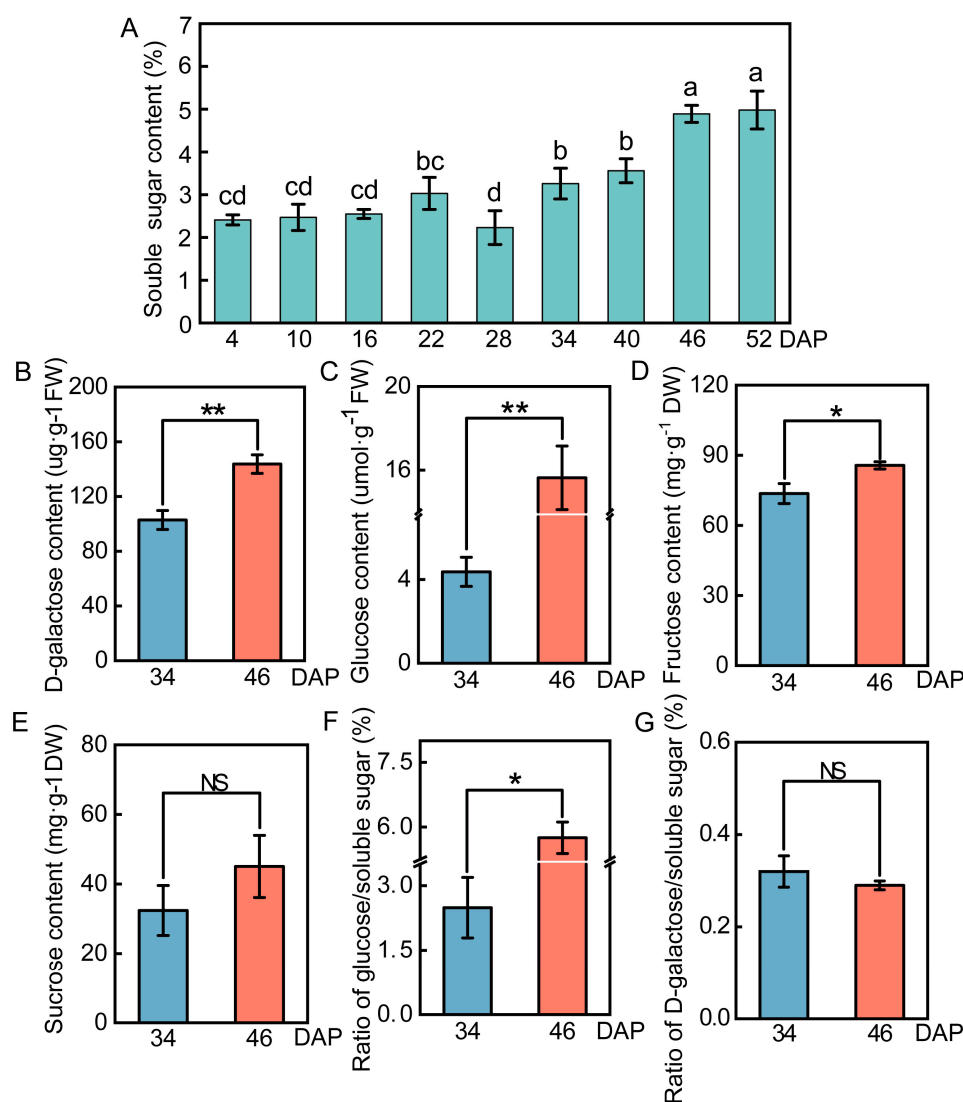


Figure 1. Sugar content in wucail leaves. (A) Soluble sugar content (%). (B) D-galactose content ($\mu\text{g}\cdot\text{g}^{-1}$ FW). (C) Glucose content ($\mu\text{mol}\cdot\text{g}^{-1}$ FW). (D) Fructose content ($\text{mg}\cdot\text{g}^{-1}$ DW). (E) Sucrose content ($\text{mg}\cdot\text{g}^{-1}$ DW). (F) Ratio of glucose/soluble sugar. (G) Ratio of D-galactose in/soluble sugar. FW and DW meant fresh weight and dry weight, respectively. Values presented are the mean \pm SE ($n \geq 3$), and bars with different letters represent significant differences at $p < 0.05$. * and ** meant $p < 0.05$ and $p < 0.01$, respectively. NS indicated no significant difference.

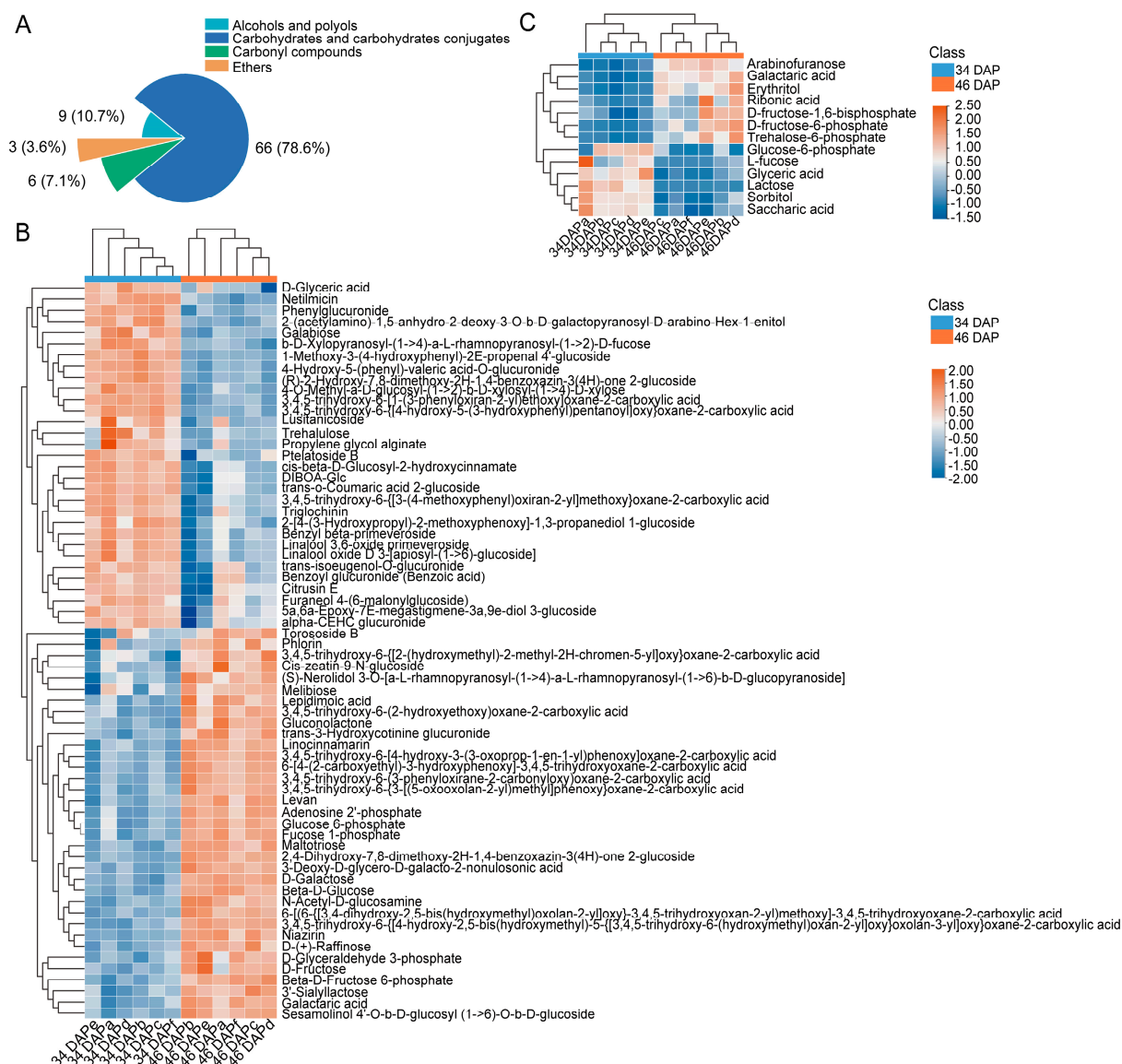


Figure 2. Classification and heatmap of DAMs in wucai leaves. **(A)** Classification of organooxygen compounds in each sub class category in LC-MS/MS. **(B,C)** Heatmap of DAMs as carbohydrates and carbohydrate conjugates in LC-MS/MS and GC-MS/MS. The data were derived from the numbers of DAMs in each sub-class category in the LC-MS/MS and GC-MS/MS analyses.

2.3. Kyoto Encyclopedia of Genes and Genomes (KEGG) Enrichment Analysis of DAMs Related to Sugar Accumulation in Wucai Leaves

To identify the major pathways of DAMs related to sugar accumulation in wucai leaves, KEGG enrichment analysis was conducted. The *p*-value in the pathways indicates the significance and Rich factor derived from ratio of DAMs/total metabolite number in the pathway. The LC-MS/MS analysis showed that DAMs related to sugar accumulation were notably enriched in the pentose phosphate pathway (ath00030), galactose metabolism (ath00052), glycolysis/gluconeogenesis (ath00010), and fructose and mannose metabolism (ath00051) pathways (Figure 3A). In the GC-MS/MS analysis, DAMs related to sugar accumulation were notably enriched in galactose metabolism (ath00052) and starch and sucrose metabolism (ath00500) (Figure 3B). It was interesting that the enrichment pathways in LC-MS/MS and GC-MS/MS were somewhat distinct. The reason could be due to the variation in quantities of other DAMs detected in the LC-MS/MS and GC-MS/MS analyses.

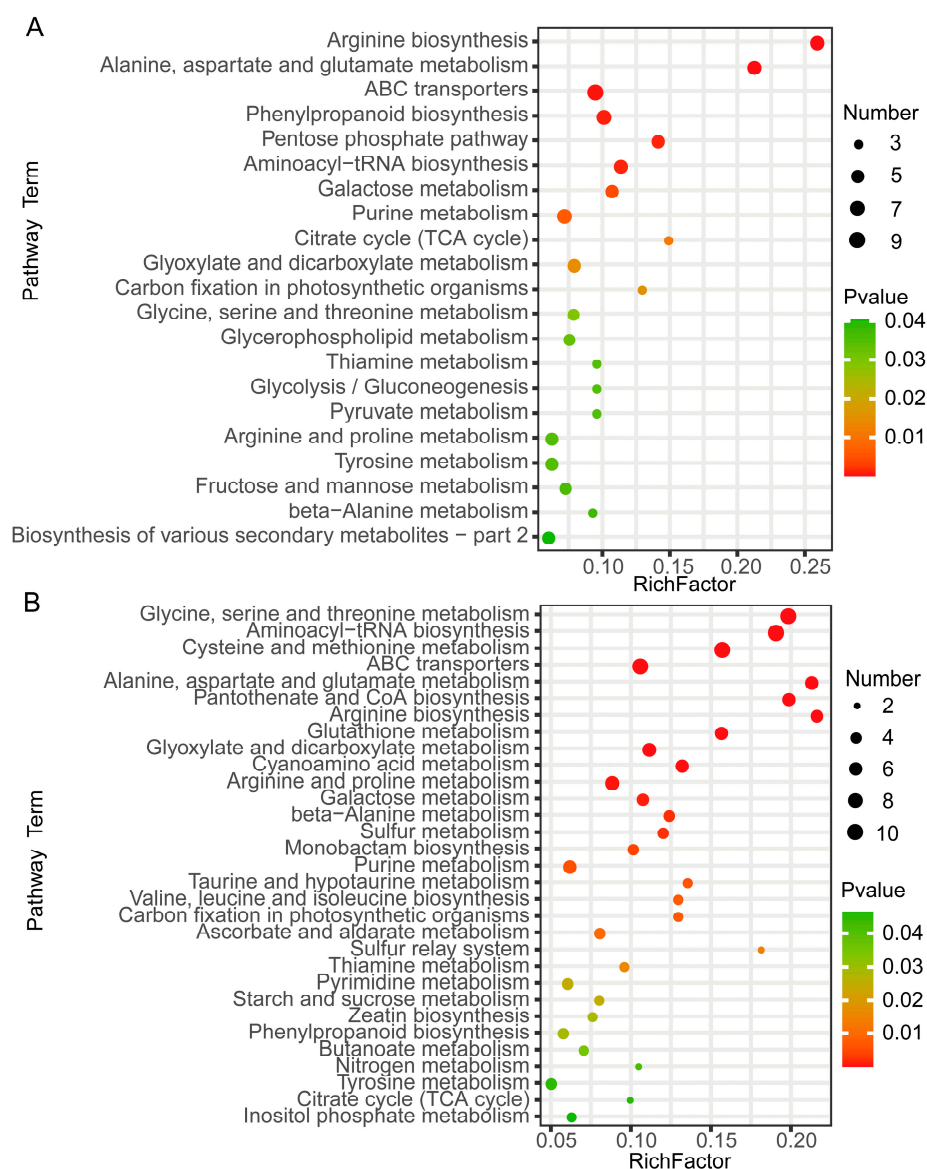


Figure 3. Enriched KEGG pathways with DAMs based on p -value < 0.05. (A) LC-MS/MS. (B) GC-MS/MS. The abscissa represents the rich factor: DAMs/total DAMs number. The size of the dot indicates the number of DAMs.

2.4. Biomarkers Analysis Related to Sugar Accumulation

In the DAM analysis, we found that many carbohydrates and carbohydrate conjugates were upregulated. However, the major sugars involved in sugar accumulation in wucai were still unclear. OPLS-DA, a supervised discriminant analysis statistical method, was used to intuitively identify the differences between samples. The VIP score was obtained according to the OPLS-DA model, and potential biomarkers were distinguished with $VIP > 1$. We found that the numbers and fold-change of the DAMs related to sugar accumulation in the GC-MS/MS analysis were generally lower than those of the LC-MS/MS analysis. Consequently, OPLS-DA S-plot analysis based on the LC-MS/MS data was performed to identify significant DAMs and potential biomarkers. A total of 17 DAMs identified as biomarker candidates were filtered in the OPLS-DA S-plot (Supplementary Figure S4 and Supplementary Table S3). Of the candidates, the differential accumulation of β -D-glucose, D-galactose, and trehalose was significant (Supplementary Table S3). β -D-glucose and D-galactose, which are carbohydrates and carbohydrate conjugates, were upregulated (Supplementary Table S3). In order to more rigorously assess the results and their ac-

curacy, further analysis of biomarkers was conducted using MetaboAnalyst 5.0 (<https://www.metaboanalyst.ca/>, accessed on 27 August 2021). Thirteen biomarkers were screened based on $\log_2(\text{FC})$, t-tests, and AUC (Table 1). This showed that β -D-glucose and D-galactose had excellent AUC and $\log_2(\text{FC})$ values (Figure 4). The result validated that β -D-glucose and D-galactose could indeed be the major sugars in sugar accumulation in wucaï and had positive effects on the sweetness. D-galactose also participates in amino sugar and nucleotide sugar metabolism (ath00520), and this pathway was screened for further analysis. We found that DAMs involved in enrichment pathways in the GC-MS/MS analysis were also present in the LC-MS/MS data. Thus, the DAMs in the pentose phosphate pathway (ath00030), galactose metabolism (ath00052), glycolysis/gluconeogenesis (ath00010), fructose and mannose metabolism (ath00051), starch and sucrose metabolism (ath00500), and amino sugar and nucleotide sugar metabolism (ath00520) were analyzed by making a heatmap based on the LC-MS/MS data (Figure 5A). The metabolites that accumulated significantly in these enrichment pathways were D-glycoldehyde3-phosphate, D-fructose, D-(+)-raffinose, Galactonic acid, N-acetyl-D-glucosamine, β -D-fructose 6-phosphate, β -D-Glucose, Gluconolactone, Fucose 1-phosphate, levan, and Glucose 6-phosphate.

Table 1. Biomarker screening results by using MetaboAnalyst 5.0.

Metabolites	AUC	T-Test	Log ₂ (FC)
3,4,5-trihydroxy-6-[4-hydroxy-3-(3-oxoprop-1-en-1-yl) phenoxy] oxane-2-carboxylic acid	1.0	3.9459×10^{-6}	0.98885
D-Galactose	1.0	1.9657×10^{-7}	0.94706
6-[4-(2-carboxyethyl)-3-hydroxyphenoxy]-3,4,5-trihydroxyoxane-2-carboxylic acid	1.0	3.0412×10^{-5}	0.62342
Pheophorbide a	1.0	3.2816×10^{-7}	3.142
Quinoline-3-carboxamides	1.0	6.0721×10^{-7}	-2.6307
ibandronate	1.0	3.3144×10^{-9}	1.3004
5'-Butyrylphosphouridine	1.0	2.1576×10^{-6}	-1.0662
Phosphatidyl glycerol	1.0	2.0603×10^{-9}	2.8388
Beta-D-Glucose	1.0	6.6146×10^{-7}	1.2187
(s)C(S)S-S-Methylcysteine sulfoxide	1.0	2.6679×10^{-7}	2.2726
3,4,5-trihydroxy-6-(3-phenyloxirane-2-carboxyloxy) oxane-2-carboxylic acid	1.0	5.1913×10^{-6}	0.98688
Trehalulose	1.0	9.5148×10^{-4}	-0.77498
Levan	1.0	3.2252×10^{-5}	0.9449

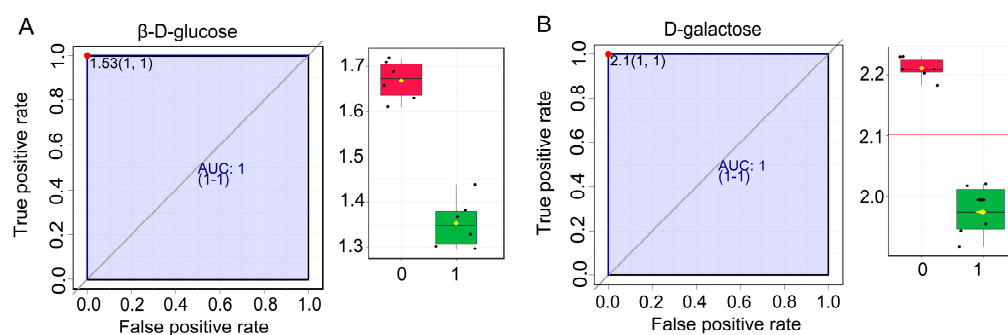


Figure 4. ROC and box plot of the biomarkers. (A) β -D-glucose. (B) D-galactose. The ROC curve closer to the left parietal corner indicates that the DAM has excellent sensitivity and specificity. The box plot intuitively shows the differences in expression abundance between the DAMs. The red box indicated 46 DAP, while the green one indicated 34 DAP.

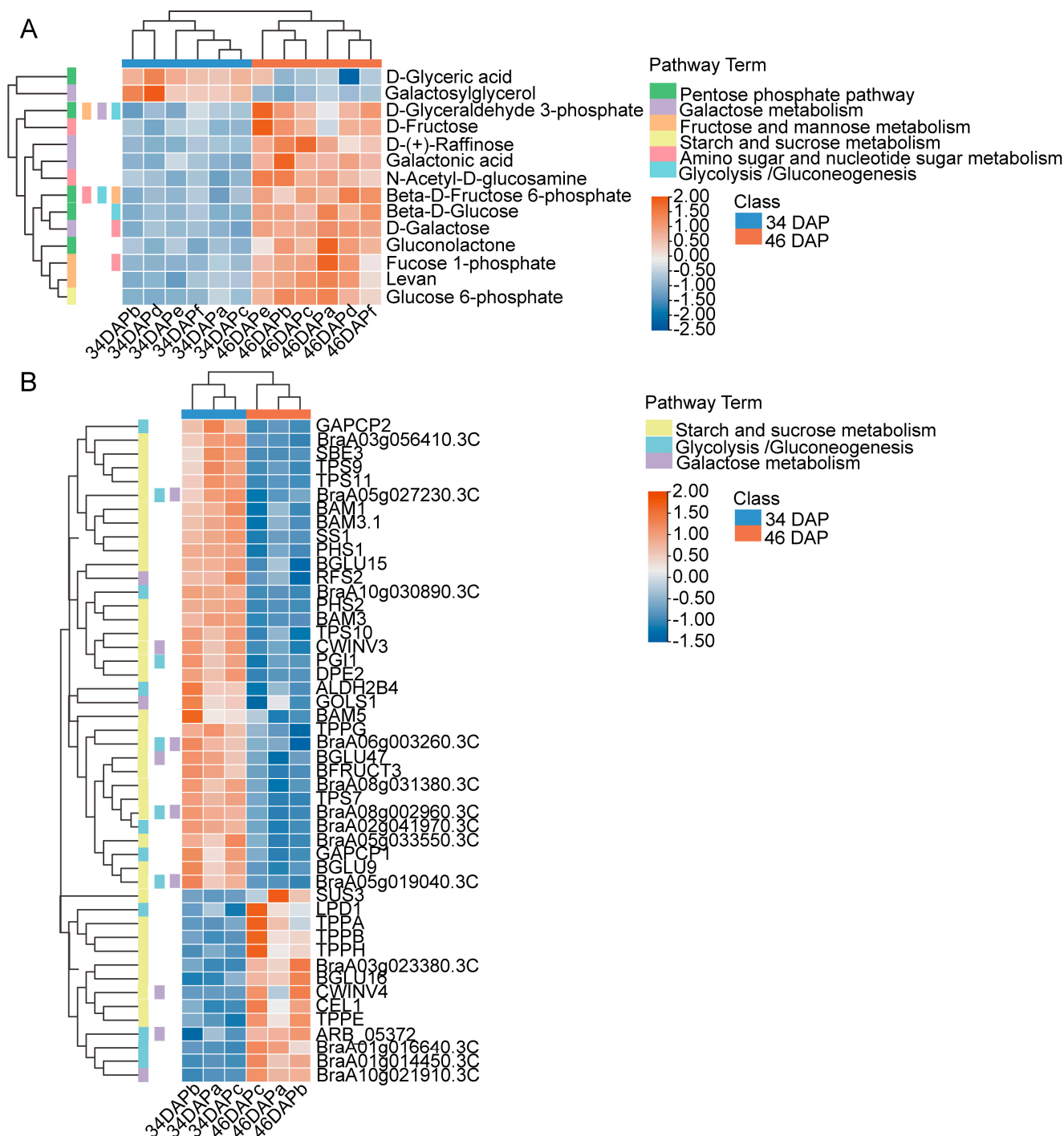


Figure 5. Heatmap of DAMs and DEGs in KEGG enrichment pathways in wucaï leaves. **(A)** Heatmap of DAMs located in KEGG enrichment pathways in the LC-MS/MS analysis. **(B)** Heatmap of DEGs in galactose metabolism, glycolysis/gluconeogenesis, and starch and sucrose metabolism. The color lump on the left of the heatmap indicates the corresponding pathways. The heatmap was based on the expression abundance of the DAMs and Fragments Per Kilobase of transcript per Million mapped reads (FPKM) values of the DEGs.

2.5. Transcriptome Analysis

Six mixed replicates of wucaï leaves at two periods (34 DAP and 46 DAP) were subjected to RNA-Seq analysis in order to identify the potential molecular mechanisms responsible for sugar accumulation in wucaï. After filtering, a total of 39.70 G of clean

data were obtained from the wucaï leaves. The Q30 (sequences with sequencing error rates lower than 0.1%) content of the six cDNA libraries were more than 92.63%, and the average GC content was 48.07% (Supplementary Table S4). Overall, the data indicated that the Illumina sequencing data were of high quality and could be used for further analysis (Supplementary Table S5).

All 4761 unigenes were searched in the Gene Ontology (GO) and KEGG databases, with 3431 and 1110 corresponding annotated unigenes. The GO term analysis of the wucaï leaf transcriptome showed that 21 terms were related to the biological process category, of which “biological regulation,” “cellular process,” “metabolic process,” and “single-organism process” were the main GO terms (Supplementary Figure S5). Thirteen terms were correlated with the cellular component category, of which “cell,” “cell part,” and “organelle” were the most abundant GO terms. Twelve terms were included in the molecular function category, of which “binding” and “catalytic activity” made major contributions. In addition, 18 KEGG pathways were annotated, among which “carbohydrate metabolism,” “translation,” and “signal transduction” were the most abundant KEGG pathways (Supplementary Figure S6).

2.6. Coexpression Analysis of Genes Related to D-Galactose and β -D-Glucose Accumulation

The major sugars involved in sugar metabolism in wucaï are D-galactose and β -D-glucose. To explore the metabolic differences in the two sugars at the sugar transformation periods, the accumulation of the two sugars was analyzed by combined transcriptome and metabolome analysis. D-galactose and β -D-glucose were mainly involved in the galactose metabolism (brp00052), glycolysis/Gluconeogenesis (brp00010), and starch and sucrose metabolism (brp00500) pathways, and, thus, we focused on DEGs related to these three metabolic pathways. It was found that most genes related to starch degradation and synthesis, trehalose synthesis, and phosphorylating D-fructose, D-glucose, and β -D-glucose were downregulated (Figure 5B). The downregulated DEGs mainly included *BAM* (β -amylase), *DPE* (4- α -glucanotransferase), *PHS* (α -glucan phosphorylase), *SS* (starch synthase), *SBE* (1,4- α -glucan-branching enzyme), *TPS* (α - α -trehalose-phosphate synthase), *TPP* (trehalose-phosphate phosphatase), and other genes (hexokinase).

According to the major two sugars and related DEGs, we constructed an accumulation pathway of D-galactose and β -D-glucose (Figure 6A). In this way, there were three DEGs encoding INV, namely *CWINV3*, *CWINV4* and *VINV* (*BRFUCT3*), all of which encode AI. Of these genes, only the expression of *CWINV4* was up-regulated. Raffinose and stachyose located in the galactose metabolic pathway were decomposed into D-galactose under AI (*CWINV4*). In the meantime, raffinose and stachyose were hydrolyzed into D-glucose under the action by the same gene. *CWINV4* was also present in the starch and sucrose metabolic pathway, converting sucrose to D-glucose by hydrolysis. Moreover, cellulose in the starch and sucrose metabolic pathway was hydrolyzed to generate D-glucose. There were six DEGs associated with cellulose hydrolysis, EG (*BraA03g023380.3C*, *CEL1*) was up-regulated, while only one (*BGLU16*) of the BGL DEGs (*BGLU16*, *BGLU9*, *BGLU15*, and *BGLU47*) was up-regulated. Under the synergistic effect of *BraA03g023380.3C*, *CEL1*, and *BGLU16*, cellulose was gradually hydrolyzed into D-glucose. Aldose 1-epimerase (AEP) was able to catalyze the conversion of D-glucose to β -D-glucose. The generated D-glucose was converted to β -D-glucose by up-regulated expression of *ARB_05372* (AEP). HK could phosphorylate β -D-glucose to β -D-Glucose 6-phosphate (β -D-glucose 6P), which later entered the glycolysis pathway. The four HK DEGs identified in this paper (*BraA06g003260.3C*, *BraA08g002960.3C*, *BraA05g019040.3C*, and *BraA05g027230.3C*) were all down-regulated, reducing the phosphorylation of β -D-glucose and promoting the accumulation of the sugar. The genes (galactokinase) catalyzing D-galactose were not differentially expressed, which showed that the accumulation of D-galactose mainly depended on AI under the action of *CWINV4* during the maturation process of wucaï. In the transcriptome analysis, the FPKM value of *CWINV4* at 34 DAP was zero. Hence, the relative expression of *CWINV4* in the roots, stems, leaves, and petioles at 34 DAP and 46 DAP was detected. The relative

expression of *CWINV4* at 46 DAP was generally higher than that at 34 DAP in the four tissues, especially in the leaves and petioles (Supplementary Figure S7).

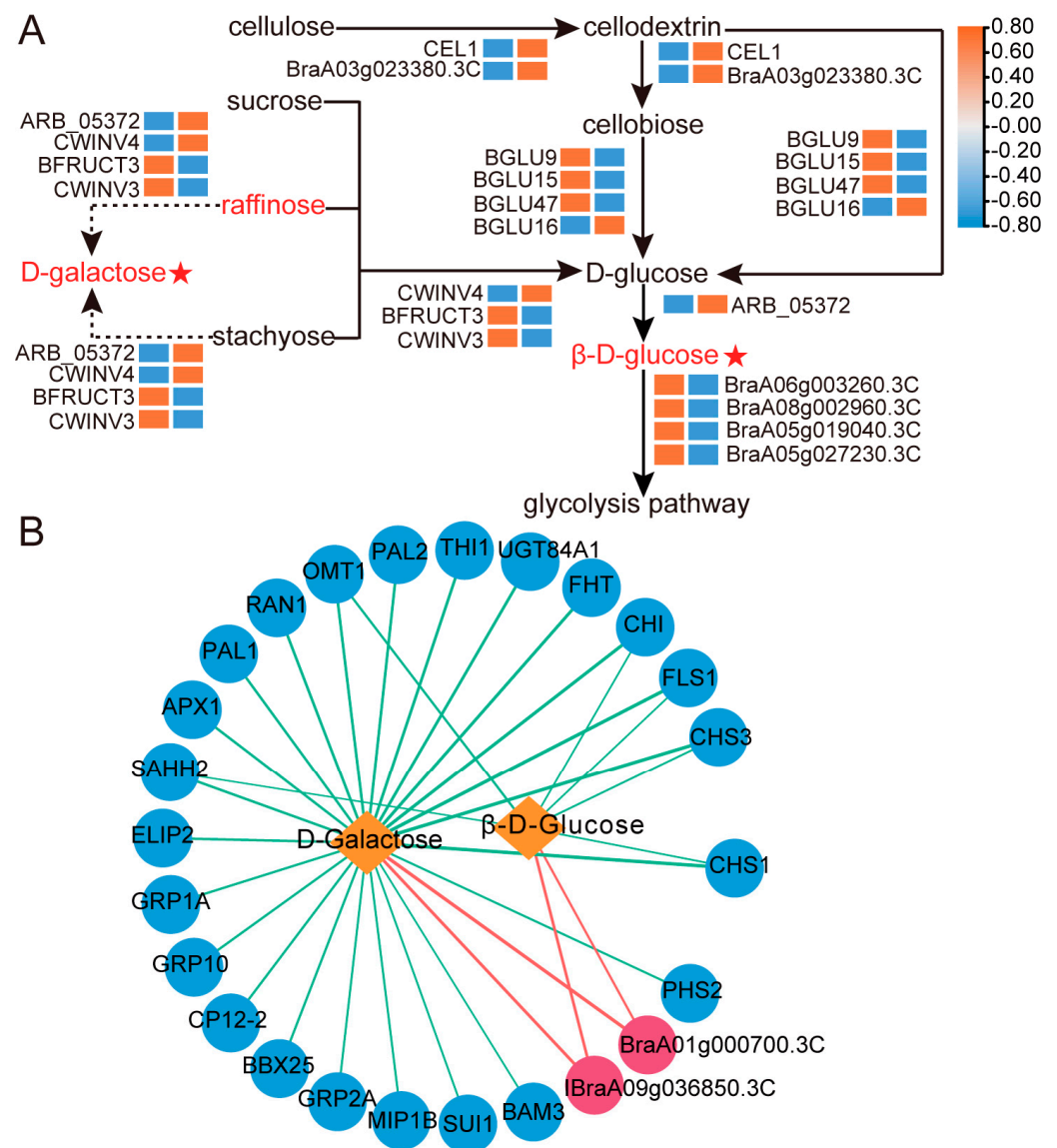


Figure 6. Accumulation pathway and Interact network of D-galactose and β-D-glucose. (A) Accumulation pathway. Metabolites upregulated or undifferentiated at 46 DAP are indicated in red and black. The red asterisk indicates a biomarker. The left and right columns of the heatmap represent 34 DAP and 46 DAP, respectively. Genes upregulated or downregulated are shown in orange and blue, respectively. The heatmap was based on the FPKM values of the DEGs. (B) Interact network. The circles with red and blue represent up-regulated and down-regulated DEGs, respectively. The orange diamond shape represents the two main accumulated sugars. The positive and negative correlations are represented by red and green lines, respectively. The thicker the line, the higher the correlation.

To explore other genes that contribute to the accumulation of D-galactose and β-D-glucose, we selected TOP100 DEGs in the transcriptome and calculated the correlation between the expression of DEGs and response intensity data of biomarkers using the Pearson correlation method. DEGs with correlation values ≥ 0.98 or ≤ -0.98 and $p < 0.05$ were selected and an interaction network was produced (Figure 6B). These were 26 and 8 DEGs that were significantly associated with D-galactose and β-D-glucose, respectively. *BraA09g036850.3C* and *BraA01g000700.3C* had a significant positive correlation with both D-galactose and β-D-glucose (Figure 6B). The DEGs with a significant negative correlation

with β -D-glucose were *SAHH2* (adenosylhomocysteinase 2), *CHI* (chalcone-flavonone isomerase), *CHS1* (chalcone synthase 1), *CHS3* (chalcone synthase 3-like), *FLS1* (flavonol synthase/flavanone 3-hydroxylase), and *OMT1* (flavone 3'-O-methyltransferase 1-like), which also had a significant negative correlation with D-galactose (Figure 6B).

2.7. Changes in Relative Expression Levels of DEGs and Enzyme Activities

Twenty DEGs in the KEGG pathways and eight DEGs significantly associated with both D-galactose and β -D-glucose were selected and we measured their relative expression levels at 34 DAP, 37 DAP, 40 DAP, 43 DAP, and 46 DAP (Figure 7). The changes in the relative expression level of these genes at 46 DAP vs. 34 DAP were consistent with the transcriptome data (Figures 6 and 7). The relative expression levels of *CWINV4*, *BraA03g023380.3C*, *BGLU16*, and *ARB_05372* showed an increasing trend from 40 DAP and peaked at 46 DAP (Figure 7). *CWINV3*, *BGLU9*, *BGLU15*, *BGLU47*, *BraA06g003260.3C*, *BraA05g027230.3C*, *BraA05g019040.3C*, *BAM1*, *BAM3-like*, *SAHH2*, *CHI*, and *FLS1* were genes that were downregulated in the transcriptome, generally peaking at 37 DAP or 40 DAP and continuing to be downregulated until 46 DAP (Figure 7). *CEL1*, *SUS3*, and *BraA01g000700.3C* had irregularly varying relative expression levels, but the highest expression was observed at 46 DAP (Figure 7). Although *BraA09g036850.3C* was upregulated around maturation, its expression level peaked at 37 DAP (Figure 7). These results suggested that these DEGs may function at different stages.

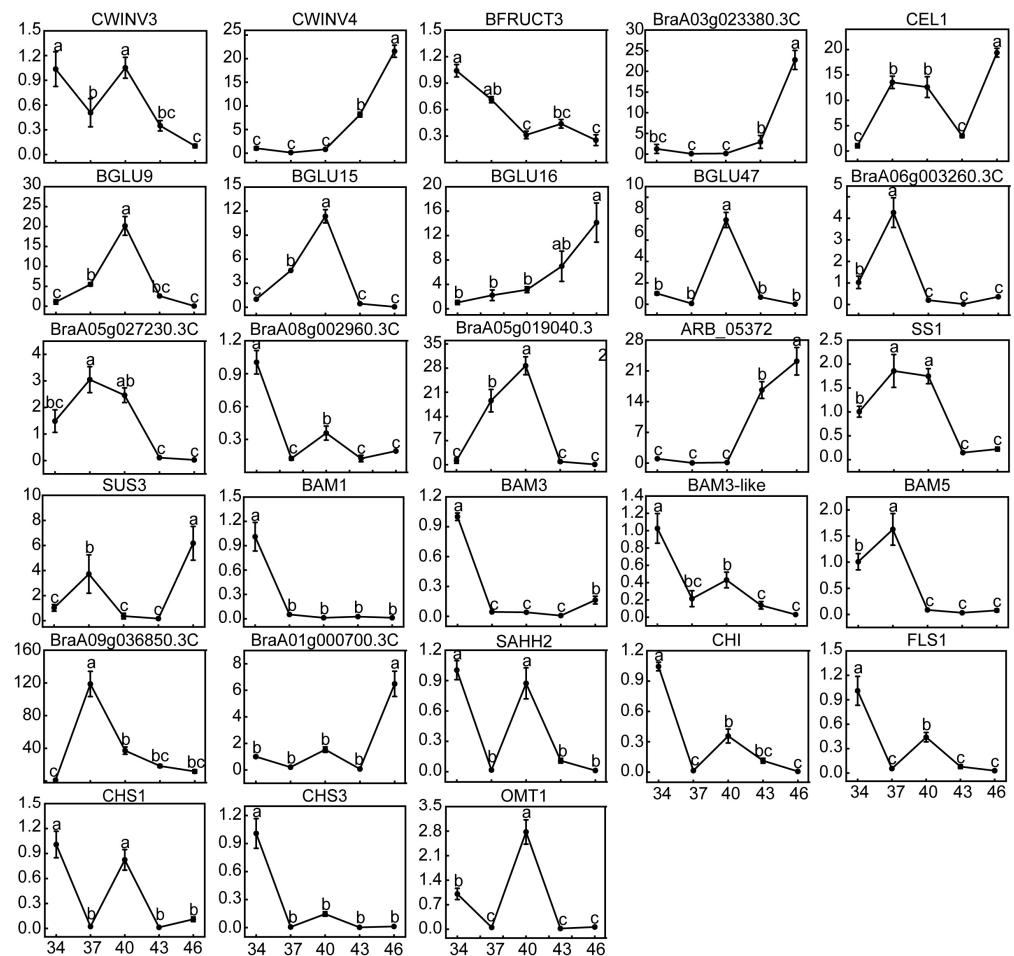


Figure 7. Relative expression level of DEGs during wucai ripening. The values obtained by the quantitative real-time PCR (qRT-PCR) represent the mean \pm SE of three replicates. Bars with different letters are significantly different at $p < 0.05$.

To understand whether the enzymes encoded by these genes play a role in sugar accumulation, we determined eight enzyme activities at 34 DAP and 46 DAP due to problems with the assay of some enzymes. The activities of CL, AI, and SUS were significantly increased, consistent with the up-regulated expression of *CWINV4*, *BraA03g023380.3C*, *CEL1*, *BGLU16*, and *SUS3* (Figures 7 and 8B,D,E). Similarly, the down-regulation of *BraA06g003260.3C*, *BraA08g002960.3C*, *BraA05g019040.3C*, *BraA05g027230.3C*, *BAM1*, *BAM3*, *BAM3-like*, *BAM5*, *CHS1*, and *CHS3* resulted in a significant decrease in the activities of HK, β -amylase (BMY), and chalcone synthase (CHS) (Figure 7). The activity of α -amylase (AMY) and SPS at 46 DAP was close to that at 34 DAP, and DEGs encoding these two enzymes also did not appear in our transcriptome data (Figures 5B and 8C,G). In general, the significant increase in AI and CL activities promoted sugar biosynthesis, while the significant decrease in BMY, HK, and CHS activities suppressed sugar loss.

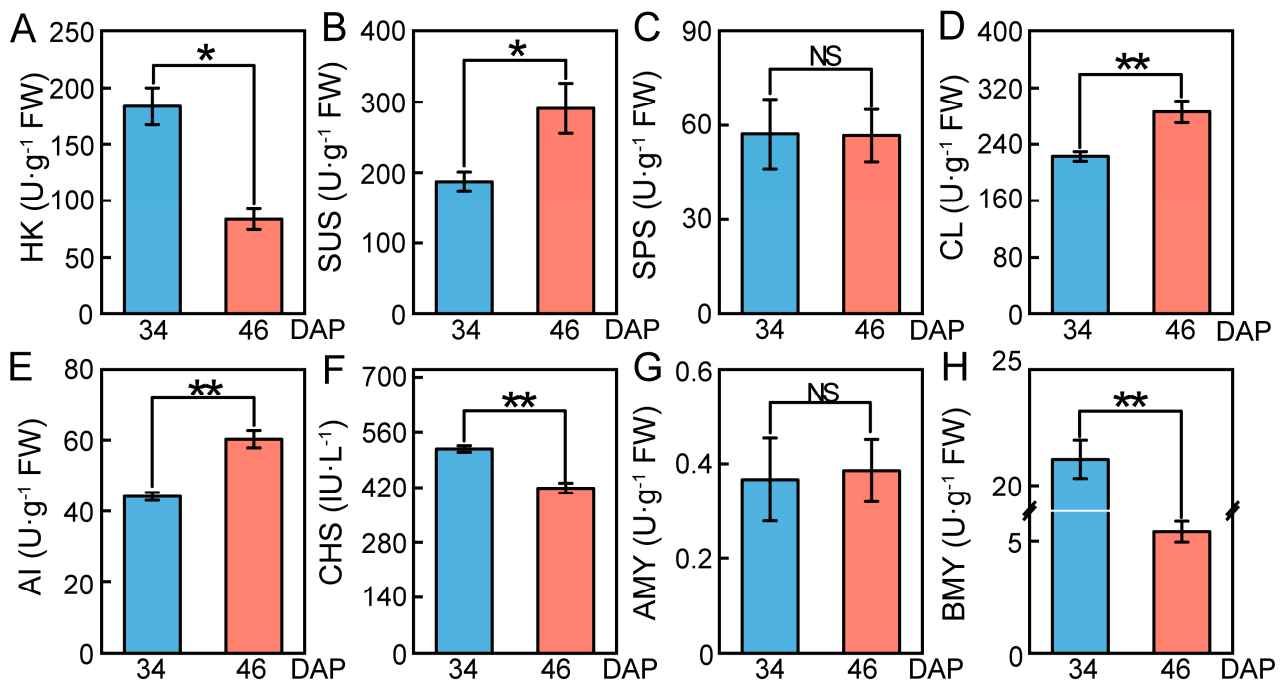


Figure 8. Enzyme activities in wucai leaves at 34 DAP and 46 DAP. (A) Hexokinase (U·g⁻¹ FW). (B) Sucrose synthase (U·g⁻¹ FW). (C) Sucrose phosphate synthase (U·g⁻¹ FW). (D) Cellulase (U·g⁻¹ FW). (E) Acid convertase (U·g⁻¹ FW). (F) Chalcone synthase (IU·L⁻¹). (G) α -amylase (U·g⁻¹ FW). (H) β -amylase (U·g⁻¹ FW). Values presented are the mean \pm SE (n \geq 3), * p < 0.05, ** p < 0.01 and NS indicated no significant difference between bars.

3. Discussion

Sugar regulatory pathways are vital for metabolism during vegetable and fruit development and maturation [33]. The sweetness of vegetables and fruit depends mainly on the type and composition of sugars, which play key roles in flavor [10,48]. Sweetness, as an important indicator of wucai quality, increased significantly during the sugar maturation process. As research on sugar accumulation in wucai is limited, the sugar composition, sugar changes, and expression of genes related to sugar accumulation were analyzed during sugar transformation in wucai “W16-19-5” herein.

As previously reported in Chinese cabbage, tomato, pumpkin, watermelon, and melon, a significant increase in soluble sugars occurred during ripening [28,34,42,49–51]. In our study, the change in soluble sugar in wucai was similar to those in the above fruit and vegetables during the maturation process. In addition, we found that the soluble sugar content at 28 DAP was relatively low compared to at 22 DAP (Figure 1A). Wucai is grown in autumn and winter, and the air temperature gradually decreases after sowing. The growth environment of wucai was simulated in a growth chamber herein, and lowering of the

temperature was first initiated at 28 DAP. Thus, we inferred that the soluble sugar decreased at 28 DAP due to the change in temperature. The growth environment of wheat is similar to that of wucai, and D-galactose accumulated greatly at the late stage of development in wheat [52]. D-galactose, in addition to sucrose, glucose, and fructose, in wucai was measured at 34 DAP and 46 DAP. We found that sucrose did not increase significantly, whereas glucose and D-galactose did more than fructose.

Compared to 34 DAP, the ratio of glucose/soluble sugar increased significantly at 46 DAP (Figure 1F). Though there were no differences between the ratio of D-galactose/soluble sugar at the two periods, a great increase in their content occurred (Figure 1B,G). Carbohydrates also mainly constitute the differential metabolites during the ripening of kiwifruit and watermelon, which is consistent with our results [53,54]. In grape berry, sorghum stem, saffron corm, and melon, metabolites related to sugar accumulation were mainly enriched in fructose and mannose metabolism, starch and sucrose metabolism, glycolysis/gluconeogenesis, and pentose phosphate pathways [51,55–57]. We found that in addition to the pathways described above, galactose metabolism was also a significantly enriched pathway (Figure 3). The results showed that D-galactose and β -D-glucose were indeed the major accumulated sugars during the sugar transformation process and played a critical role in sugar accumulation.

Sweetness, one of the major traits of wucai, is a significant factor influencing wucai quality and is also an indicator of consumer preference [3]. In this study, we found that D-galactose and β -D-glucose, which have a sweet taste, were the major sugars in the sugar accumulation process in wucai (Table 1 and Figure 4). Therefore, the mechanism of accumulation of the two major sugar was analyzed using transcriptomics.

AI promoted the hydrolysis of not only sucrose, but also raffinose and stachyose [26]. CWINV and VINV activities were positively regulated by their encoding genes and they all were the AI [26–28]. The downregulation of *BFRUCT3* showed that sugar accumulation did not depend on the hydrolysis of sucrose in the vacuoles during wucai ripening. Thus, the up-regulation of *CWINV4* during the ripening of wucai resulted in a significant increase in AI activity, allowing for more D-galactose and β -D-glucose production. Wucai leaf is both the source tissue and the sink tissue. We found that the expression of *CWINV4* was significantly increased in wucai leaf compared to the other tissues at 46 DAP (Supplementary Figure S7). This result was contrary to that of Chinese cabbage [5,42]. The IM is the main tissue of sugar accumulation in Chinese cabbage. *CWIN1* (*CWINV*), *NIN-like* (*CINV*), and *VIN4b* (*VINV*) had relatively lower expressions in the inner leading leaves than the external leading leaves during Chinese cabbage ripening, especially in IM [5]. Three INV genes (encoding β -fructofuranosidase 1, β -fructofuranosidase 6, and β -fructofuranosidase 3) were also significantly downregulated in the inner leaves of yellow-head Chinese cabbage [42]. In addition, the basic leucine zipper (bZIP) transcription factor (TF) GmbZIP123 promoted the expression of three CWINV genes (*CWINV1*, *CWINV3*, and *CWINV6*) by directly binding to their promoters, resulting in higher levels of glucose, fructose, and sucrose in soybean [58]. A pitaya WRKY TF *HpWRKY3* was associated with fruit sugar accumulation via the activation of the sucrose metabolic gene *HpINV2* [59]. While there was no bZIP TF detected herein, WRKY TFs were detected in this study. Identifying which WRKY TFs can work with *CWINV4* needs further analysis and verification.

The SPS activity did not change during the maturation of wucai, but SUS activity increased remarkably. In addition, one DEG (*SUS3*) encoding SUS was up-regulated in the transcriptome data, and no SPS DEGs were found, consistent with the enzyme activities (Figures 8B,C and 5B). Therefore, it was inferred that *SUS3* promoted the synthesis of sucrose to offset the hydrolysis of sucrose under *CWINV4*. Starch degradation during ripening is a key additional process for D-glucose accumulation in fruit and is catalyzed by the action of amylases [60]. The activity of AMY and DPE increased during mango ripening with a concomitant decrease in the starch content of the fruit [13]. BMY activity and *BAMs* (*BAM1*, *BAM3*, *BAM3-like*, and *BAM5*) were significantly down-regulated (Figure 5B). *DPE* catalyzing starch conversion into D-glucose was also found to be downregulated (Figure 5B).

However, there was no differential accumulation of starch during wucaï ripening, due to the downregulation of *SS1* and *SBE3* for starch synthesis. It follows that the accumulation of β -D-glucose did not originate from starch degradation during wucaï ripening.

The cellulose hydrolytic enzyme beta-1, 4-endoglucanase (E1) gene, from the thermophilic bacterium *Acidothermus cellulolyticus*, was overexpressed in rice through *Agrobacterium*-mediated transformation [61]. Hydrolysis of transgenic rice straw yielded 43% more reducing sugars than wild-type rice straw did [61]. It was found that overexpression of *EG* promoted the hydrolysis of cellulose, which is consistent with our study. Additionally, the up-regulated expression of BGL genes in a ripe rich-sugar mango variety showed that the genes could promote the accumulation of sugar [13]. There were no CBH DEGs detected in our transcriptome data (Figure 5B). However, we observed a significant increase in CL activity. It was inferred that *CEL1* and *BraA03g023380.3C* combined with *BGLU16* catalyzed cellulose into β -D-glucose. A β -glucosidase from *Clostridium cellulovorans* (CcBG) was fused with cellulosomal endoglucanase CelD (CtCD) from *Clostridium thermocellum* [62]. CtCD CcBG showed favorable specific activities on phosphoric-acid-swollen cellulose (PASC), with greater glucose production (2-fold) when compared with a mixture of the single enzymes, further supporting our conclusions [62]. The transcription levels in mature Chinese cabbage and rich-sugar mango were significantly higher than those of unmaturing Chinese cabbage and low-sugar mango, which proved that the downregulated expression of *HK* led to the accumulation of more glucose [13,41]. Significantly reduced *HK* activity during maturation of wucaï was accompanied by the down-regulated expression of *HK* DEGs (*BraA06g003260.3C*, *BraA08g002960.3C*, *BraA05g019040.3C*, and *BraA05g027230.3C*), which reduced the loss of D-glucose and led to more conversion of D-glucose to β -D-glucose. Similarly, the downregulation of *HK* activity reduced the phosphorylation of β -D-glucose, thereby promoting sugar accumulation.

We screened 26 DEGs possibly related to D-glucose and β -D-glucose accumulation by calculating the correlation between TOP100 DEGs in transcriptome and target metabolites. Interferon-related developmental regulator (IFRD) was mainly involved in plant salt tolerance, cold tolerance, and the ABA signal transduction pathway in previous reports [63–65]. As wucaï gradually matured, the relative expression levels of *BraA09g036850.3C* were higher than those at 34 DAP, suggesting that the high expression of the gene during this process may promote sugar accumulation (Figure 7). Some scholars have pointed out the beneficial role of inositol in promoting sugar accumulation [66]. In the biosynthesis of inositol, the rate-limiting step is catalyzed by inositol-3-phosphate synthase (ISYNA) [67]. Thus, *BraA01g000700.3C* was speculated to be highly expressed after maturation to enhance sugar accumulation (Figure 7). S-adenosylhomocysteine hydrolase (SAHH) is a widespread enzyme in cells. Over-expression of *SISAHH2* could enhance SAHH enzymatic activity in tomato development and ripening stages and resulted in a major phenotypic change of reduced ripening time from anthesis to breaker [68]. Interestingly, SAHH enzyme activity levels and *SISAHH2* transcript levels appeared to be inconsistent in some tissues. For example, *SISAHH2* was not significantly elevated in transgenic fruit, but its enzymatic activity remained at a high level [68]. From the above, it was assumed that *SAHH2* decreased during the ripening process, but it still maintained a high level of enzyme activity to promote ripening and sugar accumulation in wucaï.

Sugars can be used as precursors and information-regulating molecules for synthesis of anthocyanins [69]. *CHI*, *CHS*, *FLS*, *F3H* (flavanone-3-hydroxylase), *PAL* (phenylalaninammonialyase), and *OMT1* that affect the synthesis and accumulation of anthocyanin were regulated by sugar [69,70]. For example, the expression of the petunia *CHS* gene in transgenic *Arabidopsis* leaves was induced by sugars [71]. *CHI*, *CHS*, *FLS*, and *OMT1* in wucaï were down-regulated during ripening, where the measured *CHS* activity was also significantly decreased (Figures 7 and 8). Different sugar sensing mechanisms exist in plants and respond to different sugars [72]. We speculate that in wucaï, D-galactose and β -D-Glucose could have a negative effect on the synthesis of anthocyanin, and the down-regulation of *CHI*, *CHS*, *FLS*, and *OMT1* reduced the loss of anthocyanin synthetic precursors. There

were 18 other DEGs that had a significant correlation with D-galactose, and they were all negatively correlated (Figure 6B). However, how these genes regulate sugar accumulation remains unknown, which needs the support of further studies.

This study is the first to report on sugar accumulation during the maturation process of wucai. We found that D-galactose and β -D-glucose were mainly accumulated during wucai ripening and are essential for improving the taste quality of the fruit. The upregulated expression of *CWINV4*, *CELL1*, *BGLU16*, and *BraA03g023380.3C* and downregulated expression of *BraA06g003260.3C*, *BraA08g002960.3C*, *BraA05g019040.3C*, and *BraA05g027230.3C* in the pathway might contribute to the accumulation of D-galactose and β -D-glucose. Twenty-six DEGs significantly related to D-galactose and β -D-glucose may regulate their accumulation in wucai. This research could support the quality grading of wucai and the breeding of excellent wucai lines.

4. Materials and Methods

4.1. Plant Materials and Growth Conditions

W16-19-5, a typical wucai cultivar line, was used in this study. This experiment was carried out at the breeding base of Anhui Agricultural University (Hefei, China). The seeds of the experimental variety were obtained from the Vegetable Genetics and Breeding Laboratory of Anhui Agricultural University. Seeds were sown in plugs in a greenhouse, and seedlings with 6–7 leaves were transplanted into pots containing a substrate and vermiculite at a volume ratio of 2:1. Subsequently, the seedlings were grown in a growth chamber (0 DAP) at 25 ± 1 °C (day) and 15 ± 1 °C (night) with a $300 \mu\text{mol}\cdot\text{m}^{-2}\cdot\text{s}^{-1}$ photon flux density and 70% relative humidity under a 16/8 h (day/night) photoperiod. At 28 DAP, the growth chamber was modified to 10 °C (day) and 4 °C (night), and the other conditions remained the same. The fourth and fifth fully expanded young leaves from the center of the plants, petiole, root, and stem were sampled. Fresh leaves were placed at 105 °C for 20 min and then dried at 75 °C for 24 h to obtain a dry sample. The first sampling was performed at 4 DAP and then at 5-day intervals, with sampling ending at 52 DAP (Supplementary Figure S1). Fresh samples were immediately frozen in liquid nitrogen and maintained at -80 °C for analyses.

4.2. Measurement of Sugar Content and Enzyme Activity

Measurements of soluble sugar were carried out at nine sampling periods, namely 4 DAP, 10 DAP, 16 DAP, 22 DAP, 28 DAP, 34 DAP, 40 DAP, 46 DAP, and 52 DAP. The soluble sugar was measured according to the anthrone colorimetric method with slight modifications [73]. Fresh leaves (0.2 g) were boiled in ddH₂O (10 mL) for 30 min and then filtered and homogenized (25 mL). The extract (0.5 mL) was added to 1.5 mL of ddH₂O, 0.5 mL of anthrone ethyl acetate, and 5 mL of pure sulfuric acid. The absorbance was measured at 630 nm by a UV-vis spectrophotometer (TU1950, PERSEE).

Soluble sugar, sucrose, and fructose in the dry sample were measured at 34 DAP and 46 DAP by the anthrone colorimetric method with slight modifications [73]. Dried leaves (50 mg) were mixed with 4 mL of alcohol (80%, *v/v*) and shaken at 80 °C for 30 min. The residue was extracted with 80% alcohol. The two mixtures were configured to determine the described sugar content. The first mixture contained 0.25 mL of extract, 0.25 mL of ddH₂O, and 50 μL of NaOH (2 mol/L) and was boiled at 90 °C for 5 min. The second mixture of 0.5 mL of extract and 2.5 mL of anthrone was boiled at 40 °C for 10 min. The corresponding absorbance values were measured at 620 nm. Glucose was extracted using a Solarbio reagent kit (Cat #BC1580; Beijing Solarbio Science & Technology Co., Ltd., Beijing, China). D-galactose was quantified using a kit (ADS-W-TDX046; Shanghai Kexing Trading Co., Ltd., Shanghai, China).

AI, CL, AMY, BMY, HK, SPS, and CHS activities were measured at 34 DAP and 46 DAP according to kits (Cat #BC0560, Cat #BC2540, Cat #BC2040, Cat #BC0740, Cat #BC0600, and Cat #BC0580; Beijing Solarbio Science & Technology Co., Ltd., Beijing, China. Cat #ml092866; Shanghai Enzyme-linked Biotechnology Co., Ltd., Shanghai, China), respectively.

4.3. Metabolomic Analysis

The extraction, detection, and quantitative analysis of metabolites in the samples were performed by Shanghai Lu-Ming Biotech Co., Ltd. (Shanghai, China) (<https://www.lumingbio.com/>, accessed on 3 January 2021). In brief, freeze-dried wucaï leaf samples (80 mg) were weighed and extracted overnight at $-20\text{ }^{\circ}\text{C}$ with $20\text{ }\mu\text{L}$ of 2-chloro-*l*-phenylalanine (0.3 mg/mL) dissolved in methanol as an internal standard and 1 mL of mixture of methanol and water ($7/3, v/v$). The samples were centrifuged at $13,000\text{ rpm}$ and $4\text{ }^{\circ}\text{C}$ for 15 min . The supernatants ($150\text{ }\mu\text{L}$) were collected and then filtered through $0.22\text{ }\mu\text{m}$ microfilters and transferred to LC vials. Sample extracts were filtered and analyzed by LC-MS/MS. All metabolites were identified by Progenesis QI (Waters Corporation, Milford, CT, USA) Data Processing Software, based on public databases (<http://www.hmdb.ca/>; <http://www.lipidmaps.org/>, accessed on 3 January 2021) and self-built databases. The GC-MS/MS analysis was similar to that of the LC-MS/MS analysis. Sixty milligrams of freeze-dried wucaï leaves samples was weighed and combined with $40\text{ }\mu\text{L}$ of 2-chloro-*l*-phenylalanine (0.3 mg/mL) dissolved in methanol as an internal standard and $360\text{ }\mu\text{L}$ of cold methanol. Two milliliters of chloroform and 4 mL of water were added to the sample, which was ground and then extracted. The supernatant ($200\text{ }\mu\text{L}$) was transferred to a glass sampling vial for vacuum-drying at room temperature. Eighty microliters of 15 mg/mL of methoxyamine hydrochloride in pyridine was subsequently added, following which $80\text{ }\mu\text{L}$ of BSTFA (with 1% TMCS) and $20\text{ }\mu\text{L}$ of *n*-hexane were added into the mixture after rotating for 2 min and incubating at $37\text{ }^{\circ}\text{C}$ for 90 min , which was then followed by vigorous vortexing for 2 min and then derivatization at $70\text{ }^{\circ}\text{C}$ for 60 min . After 30 min at room temperature, the sample extracts were filtered and analyzed by GC-MS/MS. Metabolites were annotated through the LUG database (Untarget database of GC-MS/MS from Lumingbio). Metabolic alterations among experimental groups were visualized by principal component analysis (PCA) and (orthogonal) partial least-squares-discriminant analysis (O)PLS-DA. Group discrimination was ascertained based on VIP scores >1 obtained from the OPLS-DA model. Metabolites with VIP > 1 and p -value < 0.05 were considered differential metabolites.

The OPLS-DA S-plot was obtained from the OPLS-DA, with minor modification. All points representing DAMs in the figure are distributed in the first and third quadrants, similar to an S-shape, which is called an OPLS-DA S-plot. Metabolites that are significantly different are distributed in the upper left corner and lower right corner. Biomarker analysis was performed by MetaboAnalyst 5.0 (<https://www.metaboanalyst.ca/>, accessed on 27 August 2021).

4.4. RNA-Seq Analysis

The total RNA of the wucaï leaf samples at the two sampling periods (34 DAP and 46 DAP) was extracted using a mirVana miRNA Isolation Kit (Ambion) according to the manufacturer's instructions. The RNA integrity was evaluated using an Agilent 2100 Bioanalyzer (Agilent Technologies, Santa Clara, CA, USA). The samples with RNA Integrity Number (RIN) ≥ 7 were subjected to subsequent analysis. The libraries were constructed using a TruSeq Stranded mRNA LTSample Prep Kit (Illumina, San Diego, CA, USA) following the manufacturer's instructions. Then, six cDNA libraries were sequenced on the Illumina sequencing platform (HiSeqTM 2500 or Illumina HiSeq X-Ten). Raw data (raw reads) were first processed using Trimmomatic [74], and then the low-quality reads were removed to obtain the clean reads for subsequent analyses. The clean reads were mapped to the *B. rapa* reference genome using HISAT2 [75]. Fragments Per Kilobase of transcript per Million mapped reads (FPKM) values and the read counts of each gene were obtained, respectively, by Cufflinks and HTSeqcount [76]. Differentially expressed unigenes (DEGs) were identified using the DESeq (2012) function estimateSizeFactors and nbinomTest, and $q < 0.05$ and $|\log_2(\text{fold change})| > 1$ were set as the threshold for significant differential expression. KEGG pathway enrichment analysis of DEGs was performed in R software based on the hypergeometric distribution.

4.5. qRT-PCR Analysis

Twenty-eight genes were selected for qRT-PCR analysis, and a gene encoding actin was used as the internal reference gene. The total RNA of the wucai leaves was extracted using an RNA kit (Takara Biomedical Technology Co., Beijing, China). The primers designed by Primer software v6.0 (Premier Biosoft International, Palo Alto, CA, USA) are listed in Supplementary Table S6. The qRT-PCR was performed using the Hieff[®] qPCR SYBR[®] Green Master Mix (No Rox) (Yeasen, Shanghai, China). The relative mRNA expression level of genes was calculated using the $2^{-\Delta\Delta CT}$ method [77].

4.6. Statistical Analysis

All data were analyzed using Origin 2020 64 Bit, Adobe Illustrator 2019, Excel 2019, Adobe Photoshop 2021, Cytoscape_v3.8.2, and SPSS 26.0 and were expressed as mean \pm SD. Tukey's post hoc test was used for mean comparisons using $p < 0.05$. All data were from three biological replications.

5. Conclusions

In the present study, LC-MS/MS, GC-MS/MS, and RNA-Seq profiling were performed to explore the molecular regulatory mechanisms of sugar accumulation during the maturity process of wucai. In the comparison of 46 DAP vs. 34 DAP, the number of DAMs associated with carbohydrates was prominent in LC-MS/MS and GC-MS/MS. The main ways of sugar accumulation were the pentose phosphate pathway, galactose metabolism, glycolysis/gluconeogenesis, starch and sucrose metabolism, and fructose and mannose metabolism in metabolome profiling. D-galactose and β -D-glucose, the two significantly accumulated metabolites, were identified as the main sugar to improving the taste quality of wucai during sugar transformation. Combined with the transcriptome data, the pathway of sugar accumulation and the interaction network of DEGs and the two sugars were generated. *CWINV4*, *CEL1*, *BGLU16*, and *BraA03g023380.3C*, which directly regulate sugar production, were significantly upregulated, and the enzymes activities (AI and CL) they encode showed the same results. Likewise, the expressions of HK (*BraA06g003260.3C*, *BraA08g002960.3C*, *BraA05g019040.3C*, and *BraA05g027230.3C*) and HK activity were both significantly decreased, reducing the metabolic loss of sugar. The 26 DEGs in the interaction network may regulate sugar accumulation through some unknown pathways. Among them, *BraA09g036850.3C*, *BraA01g000700.3C*, *SAHH2*, *CHI*, *CHS1*, *CHS3*, *FLS1*, and *OMT1* all have effects on D-galactose and β -D-glucose metabolism. These findings could help us understand the main substances and molecular regulation mechanism during the process of sugar accumulation.

Supplementary Materials: The following supporting information can be downloaded at: <https://www.mdpi.com/article/10.3390/ijms24054816/s1>.

Author Contributions: C.W. and L.Y. designed the study. J.Z. performed the experiments, analyzed the data, plotted all the figures, and wrote the paper. S.Z., X.G., Y.Y., J.H., G.C., J.W., X.T. and J.W. investigated the study and reviewed the manuscript. C.W. and L.Y. supervised the study and edited the manuscript. All authors contributed to the article and approved the submitted version. All authors have read and agreed to the published version of the manuscript.

Funding: This work was supported by the Collaborative Innovation Project of Universities in Anhui Province (GXXT-2021-054), the Graduate Scientific Research Project of Anhui Province in 2021 (YJS20210247), the National Natural Science Foundation of China (32272703), the Performance Award of Anhui Pakchoi Germplasm Resource Bank (Nursery) Project (21432003), the University Natural Science Research Project of Anhui Province (KJ2020ZD11), and the Nature Fund of Anhui Province (2008085MC80).

Institutional Review Board Statement: Not applicable.

Informed Consent Statement: Not applicable.

Data Availability Statement: The data for RNA-sequencing are available at the National Center for Biotechnology Information (NCBI) with accession number PRJNA898258. The data for Metabonomics are available in the EMBL-EBI MetaboLights database with accession number MTBLS5097 and MTBLS5096.

Conflicts of Interest: The authors declare that the research was conducted in the absence of any commercial or financial relationships that could be construed as a potential conflict of interest.

References

1. Yuan, L.; Wang, J.; Xie, S.; Zhao, M.; Nie, L.; Zheng, Y.; Zhu, S.; Hou, J.; Chen, G.; Wang, C. Comparative Proteomics Indicates That Redox Homeostasis Is Involved in High- and Low-Temperature Stress Tolerance in a Novel Wucai (*Brassica campestris* L.) Genotype. *Int. J. Mol. Sci.* **2019**, *20*, 3760. [[CrossRef](#)] [[PubMed](#)]
2. Yuan, L.; Liu, S.; Zhu, S.; Chen, G.; Liu, F.; Zou, M.; Wang, C. Comparative response of two wucai (*Brassica campestris* L.) genotypes to heat stress on antioxidative system and cell ultrastructure in root. *Acta Physiol. Plant.* **2016**, *38*, 223. [[CrossRef](#)]
3. Yuan, L.; Nie, L.; Ji, Q.; Zheng, Y.; Zhang, L.; Zhu, S.; Hou, J.; Chen, G.; Wang, C. The effect of exogenous 24-epibrassinolide pretreatment on the quality, antioxidant capacity, and postharvest life of wucai (*Brassica campestris* L.). *Food Sci. Nutr.* **2021**, *9*, 1323–1335. [[CrossRef](#)] [[PubMed](#)]
4. Wang, C.; Wang, Y.; Wang, M.; Han, H.; Luo, Y.; Ding, W.; Xu, W.; Zhong, Y.; Huang, H.; Qu, S. Soluble sugars accumulation and related gene expression during fruit development in *Cucurbita maxima* Duchesne. *Sci. Hortic.* **2020**, *272*, 109520. [[CrossRef](#)]
5. Liu, Q.; Li, J.; Liu, W. Sugar accumulation and characterization of metabolizing enzyme genes in leafy head of Chinese cabbage (*Brassica campestris* L. ssp. *pekinensis*). *Hortic. Environ. Biotechnol.* **2020**, *62*, 17–29. [[CrossRef](#)]
6. Zhang, H.; Wang, H.; Yi, H.; Zhai, W.; Wang, G.; Fu, Q. Transcriptome profiling of *Cucumis melo* fruit development and ripening. *Hortic. Res.* **2016**, *3*, 16014. [[CrossRef](#)]
7. Shammai, A.; Petreikov, M.; Yeselson, Y.; Faigenboim, A.; Moy-Komemi, M.; Cohen, S.; Cohen, D.; Besaulov, E.; Efrati, A.; Houminer, N.; et al. Natural genetic variation for expression of a SWEET transporter among wild species of *Solanum lycopersicum* (tomato) determines the hexose composition of ripening tomato fruit. *Plant J. Cell Mol. Biol.* **2018**, *96*, 343–357. [[CrossRef](#)]
8. Ko, H.Y.; Ho, L.H.; Neuhaus, H.E.; Guo, W.J. Transporter SISWEET15 unloads sucrose from phloem and seed coat for fruit and seed development in tomato. *Plant Physiol.* **2021**, *187*, 2230–2245. [[CrossRef](#)]
9. Xi, W.; Zheng, H.; Zhang, Q.; Li, W. Profiling Taste and Aroma Compound Metabolism during Apricot Fruit Development and Ripening. *Int. J. Mol. Sci.* **2016**, *17*, 998. [[CrossRef](#)]
10. Zhang, Z.; Xing, Y.; Ramakrishnan, M.; Chen, C.; Xie, F.; Hua, Q.; Chen, J.; Zhang, R.; Zhao, J.; Hu, G.; et al. Transcriptomics-based Identification and Characterization of Genes Related to Sugar Metabolism in ‘Hongshuijing’ Pitaya. *Hortic. Plant J.* **2022**, *8*, 450–460. [[CrossRef](#)]
11. Iqbal, S.; Ni, X.; Bilal, M.S.; Shi, T.; Khalil-Ur-Rehman, M.; Zhenpeng, P.; Jie, G.; Usman, M.; Gao, Z. Identification and expression profiling of sugar transporter genes during sugar accumulation at different stages of fruit development in apricot. *Gene* **2020**, *742*, 144584. [[CrossRef](#)] [[PubMed](#)]
12. Gao, L.; Zhao, S.; Lu, X.; He, N.; Zhu, H.; Dou, J.; Liu, W. Comparative transcriptome analysis reveals key genes potentially related to soluble sugar and organic acid accumulation in watermelon. *PLoS ONE* **2018**, *13*, e0190096. [[CrossRef](#)] [[PubMed](#)]
13. Li, L.; Wu, H.X.; Ma, X.W.; Xu, W.T.; Liang, Q.Z.; Zhan, R.L.; Wang, S.B. Transcriptional mechanism of differential sugar accumulation in pulp of two contrasting mango (*Mangifera indica* L.) cultivars. *Genomics* **2020**, *112*, 4505–4515. [[CrossRef](#)] [[PubMed](#)]
14. Cheng, J.; Wen, S.; Xiao, S.; Lu, B.; Ma, M.; Bie, Z. Overexpression of the tonoplast sugar transporter CmTST2 in melon fruit increases sugar accumulation. *J. Exp. Bot.* **2018**, *69*, 511–523. [[CrossRef](#)] [[PubMed](#)]
15. Wang, M.; Li, A.-M.; Liao, F.; Qin, C.-X.; Chen, Z.-L.; Zhou, L.; Li, Y.-R.; Li, X.-F.; Lakshmanan, P.; Huang, D.-L. Control of sucrose accumulation in sugarcane (*Saccharum* spp. hybrids) involves miRNA-mediated regulation of genes and transcription factors associated with sugar metabolism. *GCB Bioenergy* **2021**, *14*, 173–191. [[CrossRef](#)]
16. Gerhardt, R.; Stitt, M.; Heldt, H.W. Subcellular Metabolite Levels in Spinach Leaves: Regulation of Sucrose Synthesis during Diurnal Alterations in Photosynthetic Partitioning. *Plant Physiol.* **1987**, *83*, 399–407. [[CrossRef](#)]
17. Abdullah, M.; Cao, Y.; Cheng, X.; Meng, D.; Chen, Y.; Shakoob, A.; Gao, J.; Cai, Y. The Sucrose Synthase Gene Family in Chinese Pear (*Pyrus bretschneideri* Rehd.): Structure, Expression, and Evolution. *Molecules* **2018**, *23*, 1144. [[CrossRef](#)]
18. Huber, S.C. Role of Sucrose-Phosphate Synthase in Partitioning of Carbon in Leaves. *Plant Physiol.* **1983**, *71*, 818–821. [[CrossRef](#)]
19. Choudhury, S.R.; Roy, S.; Sengupta, D.N. A comparative study of cultivar differences in sucrose phosphate synthase gene expression and sucrose formation during banana fruit ripening. *Postharvest Biol. Technol.* **2009**, *54*, 15–24. [[CrossRef](#)]
20. Fung, R.W.M.; Langenkämper, G.; Gardner, R.C.; MacRae, E. Differential expression within an SPS gene family. *Plant Sci.* **2003**, *164*, 459–470. [[CrossRef](#)]
21. Geigenberger, P.; Reimholz, R.; Deiting, U.; Sonnewald, U.; Stitt, M. Decreased expression of sucrose phosphate synthase strongly inhibits the water stress-induced synthesis of sucrose in growing potato tubers. *Plant J. Cell Mol. Biol.* **1999**, *19*, 119–129. [[CrossRef](#)] [[PubMed](#)]

22. Zhang, X.; Wang, W.; Du, L.; Xie, J.; Yao, Y.; Sun, G. Expression Patterns, Activities and Carbohydrate-Metabolizing Regulation of Sucrose Phosphate Synthase, Sucrose Synthase and Neutral Invertase in Pineapple Fruit during Development and Ripening. *Int. J. Mol. Sci.* **2012**, *13*, 9460–9477. [[CrossRef](#)] [[PubMed](#)]
23. Wongmetha, O.; Ke, L.-S.; Liang, Y.-S. The changes in physical, bio-chemical, physiological characteristics and enzyme activities of mango cv. Jinhwang during fruit growth and development. *Chem. Chem.* **2015**, *72–73*, 7–12. [[CrossRef](#)]
24. Li, M.; Feng, F.; Cheng, L. Expression Patterns of Genes Involved in Sugar Metabolism and Accumulation during Apple Fruit Development. *PLoS ONE* **2012**, *7*, e33055. [[CrossRef](#)] [[PubMed](#)]
25. Islam, M.Z.; Hu, X.-M.; Jin, L.-F.; Liu, Y.-Z.; Peng, S.-A. Genome-Wide Identification and Expression Profile Analysis of Citrus Sucrose Synthase Genes: Investigation of Possible Roles in the Regulation of Sugar Accumulation. *PLoS ONE* **2014**, *9*, e113623. [[CrossRef](#)] [[PubMed](#)]
26. Iraqi, D.; Tremblay, F.M. Analysis of carbohydrate metabolism enzymes and cellular contents of sugars and proteins during spruce somatic embryogenesis suggests a regulatory role of exogenous sucrose in embryo development. *J. Exp. Bot.* **2001**, *52*, 2301–2311. [[CrossRef](#)]
27. Burger, Y.; Schaffer, A.A. The contribution of sucrose metabolism enzymes to sucrose accumulation in *Cucumis melo*. *J. Am. Soc. Hortic. Sci.* **2007**, *132*, 704–712. [[CrossRef](#)]
28. Zhang, X.S.; Feng, C.Y.; Wang, M.N.; Li, T.L.; Liu, X.; Jiang, J. Plasma membrane-localized SISWEET7a and SISWEET14 regulate sugar transport and storage in tomato fruits. *Hortic. Res.* **2021**, *8*, 186. [[CrossRef](#)]
29. De Coninck, B.; Le Roy, K.; Francis, I.; Clerens, S.; Vergauwen, R.; Halliday, A.M.; Smith, S.M.; Van Laere, A.; Van den Ende, W. Arabidopsis AtcwINV3 and 6 are not invertases but are fructan exohydrolases (FEHs) with different substrate specificities. *Plant Cell Environ.* **2005**, *28*, 432–443. [[CrossRef](#)]
30. Xu, D.-P.; Sung, S.-J.S.; Black, C.C. Sucrose Metabolism in Lima Bean Seeds. *Plant Physiol.* **1989**, *89*, 1106–1116. [[CrossRef](#)]
31. Dai, N.; Schaffer, A.; Petreikov, M.; Shahak, Y.; Giller, Y.; Ratner, K.; Levine, A.; Granot, D. Overexpression of Arabidopsis Hexokinase in Tomato Plants Inhibits Growth, Reduces Photosynthesis, and Induces Rapid Senescence. *Plant Cell* **1999**, *11*, 1253. [[CrossRef](#)] [[PubMed](#)]
32. Saminathan, T.; García, M.; Ghimire, B.; Lopez, C.; Bodunrin, A.; Nimmakayala, P.; Abburi, V.L.; Levi, A.; Balagurusamy, N.; Reddy, U.K. Metagenomic and Metatranscriptomic Analyses of Diverse Watermelon Cultivars Reveal the Role of Fruit Associated Microbiome in Carbohydrate Metabolism and Ripening of Mature Fruits. *Front. Plant Sci.* **2018**, *9*, 4. [[CrossRef](#)] [[PubMed](#)]
33. Umer, M.J.; Bin Safdar, L.; Gebremeskel, H.; Zhao, S.J.; Yuan, P.L.; Zhu, H.J.; Kaseb, M.O.; Anees, M.; Lu, X.Q.; He, N.; et al. Identification of key gene networks controlling organic acid and sugar metabolism during watermelon fruit development by integrating metabolic phenotypes and gene expression profiles. *Hortic. Res.* **2020**, *7*, 193. [[CrossRef](#)] [[PubMed](#)]
34. Gong, C.S.; Zhu, H.J.; Lu, X.Q.; Yang, D.D.; Zhao, S.J.; Umer, M.J.; He, N.; Yuan, P.L.; Anees, M.; Diao, W.N.; et al. An integrated transcriptome and metabolome approach reveals the accumulation of taste-related metabolites and gene regulatory networks during watermelon fruit development. *Planta* **2021**, *254*, 35. [[CrossRef](#)]
35. Wang, X.; Rong, L.; Wang, M.; Pan, Y.; Zhao, Y.; Tao, F. Improving the activity of endoglucanase I (EGI) from *Saccharomyces cerevisiae* by DNA shuffling. *RSC Adv.* **2017**, *7*, 46246–46256. [[CrossRef](#)]
36. Sutarlie, L.; Yang, K.L. Hybrid cellulase aggregate with a silica core for hydrolysis of cellulose and biomass. *J. Colloid Interface Sci.* **2013**, *411*, 76–81. [[CrossRef](#)]
37. Wang, X.; Wu, Y.; Zhou, Y. Transglycosylation, a new role for multifunctional cellulase in overcoming product inhibition during the cellulose hydrolysis. *Bioengineered* **2017**, *8*, 129–132. [[CrossRef](#)]
38. Cass, L.G.; Kirven, K.A.; Christoffersen, R.E. Isolation and characterization of a cellulase gene family member expressed during avocado fruit ripening. *Mol. Gen. Genet.* **1990**, *223*, 76–86. [[CrossRef](#)]
39. Owino, W.O.; Nakano, R.; Kubo, Y.; Inaba, A. Coordinated expression patterns of genes encoding cell wall modifying enzymes during ripening in distinct anatomical tissue regions of the fig (*Ficus carica* L.) fruit. *Postharvest Biol. Technol.* **2004**, *32*, 253–261. [[CrossRef](#)]
40. Sharma, A.; Gupta, G.; Ahmad, T.; Mansoor, S.; Kaur, B. Enzyme Engineering: Current Trends and Future Perspectives. *Food Rev. Int.* **2021**, *37*, 121–154. [[CrossRef](#)]
41. Wang, L.; Zhang, S.; Li, J.; Zhang, Y.; Zhou, D.; Li, C.; He, L.; Li, H.; Wang, F.; Gao, J. Identification of key genes controlling soluble sugar and glucosinolate biosynthesis in Chinese cabbage by integrating metabolome and genome-wide transcriptome analysis. *Front. Plant Sci.* **2022**, *13*, 1043489. [[CrossRef](#)] [[PubMed](#)]
42. Li, Y.; Fan, Y.; Jiao, Y.; Wu, J.; Zhang, Z.; Yu, X.; Ma, Y. Transcriptome profiling of yellow leafy head development during the heading stage in Chinese cabbage (*Brassica rapa* subsp. *pekinensis*). *Physiol. Plant.* **2019**, *165*, 800–813. [[CrossRef](#)] [[PubMed](#)]
43. Lin, Q.; Wang, C.; Dong, W.; Jiang, Q.; Wang, D.; Li, S.; Chen, M.; Liu, C.; Sun, C.; Chen, K. Transcriptome and metabolome analyses of sugar and organic acid metabolism in Ponkan (*Citrus reticulata*) fruit during fruit maturation. *Gene* **2015**, *554*, 64–74. [[CrossRef](#)] [[PubMed](#)]
44. Wang, R.; Shu, P.; Zhang, C.; Zhang, J.; Chen, Y.; Zhang, Y.; Du, K.; Xie, Y.; Li, M.; Ma, T.; et al. Integrative analyses of metabolome and genome-wide transcriptome reveal the regulatory network governing flavor formation in kiwifruit (*Actinidia chinensis*). *New Phytol.* **2022**, *233*, 373–389. [[CrossRef](#)]
45. Kaddurah-Daouk, R.; Kristal, B.S.; Weinshilboum, R.M. Metabolomics: A Global Biochemical Approach to Drug Response and Disease. *Annu. Rev. Pharmacol. Toxicol.* **2008**, *48*, 653–683. [[CrossRef](#)]

46. Haenisch, F.; Cooper, J.D.; Reif, A.; Kittel-Schneider, S.; Steiner, J.; Leweke, F.M.; Rothermundt, M.; van Beveren, N.J.M.; Crespo-Facorro, B.; Niebuhr, D.W.; et al. Towards a blood-based diagnostic panel for bipolar disorder. *Brain Behav. Immun.* **2016**, *52*, 49–57. [[CrossRef](#)]
47. Ahn, J.; Kim, J.; Hwang, J.; Song, J.; Kim, K.; Cha, H.-S. Urinary Metabolomic Profiling to Identify Potential Biomarkers for the Diagnosis of Behcet's Disease by Gas Chromatography/Time-of-Flight-Mass Spectrometry. *Int. J. Mol. Sci.* **2017**, *18*, 2309. [[CrossRef](#)]
48. Aslam, M.M.; Deng, L.; Wang, X.; Wang, Y.; Pan, L.; Liu, H.; Niu, L.; Lu, Z.; Cui, G.; Zeng, W.; et al. Expression patterns of genes involved in sugar metabolism and accumulation during peach fruit development and ripening. *Sci. Hortic.* **2019**, *257*. [[CrossRef](#)]
49. Abbas, H.M.K.; Huang, H.X.; Wang, A.J.; Wu, T.Q.; Xue, S.D.; Ahmad, A.; Xie, D.S.; Li, J.X.; Zhong, Y.J. Metabolic and transcriptomic analysis of two *Cucurbita moschata* germplasms throughout fruit development. *BMC Genom.* **2020**, *21*, 365. [[CrossRef](#)]
50. Dai, N.; Cohen, S.; Portnoy, V.; Tzuri, G.; Harel-Beja, R.; Pompan-Lotan, M.; Carmi, N.; Zhang, G.; Diber, A.; Pollock, S.; et al. Metabolism of soluble sugars in developing melon fruit: A global transcriptional view of the metabolic transition to sucrose accumulation. *Plant Mol. Biol.* **2011**, *76*, 1–18. [[CrossRef](#)]
51. Cheng, H.; Kong, W.P.; Tang, T.X.; Ren, K.L.; Zhang, K.L.; Wei, H.X.; Lin, T. Identification of Key Gene Networks Controlling Soluble Sugar and Organic Acid Metabolism During Oriental Melon Fruit Development by Integrated Analysis of Metabolic and Transcriptomic Analyses. *Front. Plant Sci.* **2022**, *13*, 830517. [[CrossRef](#)] [[PubMed](#)]
52. Darko, E.; Vegh, B.; Khalil, R.; Marcek, T.; Szalai, G.; Pal, M.; Janda, T. Metabolic responses of wheat seedlings to osmotic stress induced by various osmolytes under iso-osmotic conditions. *PLoS ONE* **2019**, *14*, e0226151. [[CrossRef](#)] [[PubMed](#)]
53. Liao, G.L.; Liu, Q.; Xu, X.B.; He, Y.Q.; Li, Y.Q.; Wang, H.L.; Ye, B.; Huang, C.H.; Zhong, M.; Jia, D.F. Metabolome and Transcriptome Reveal Novel Formation Mechanism of Early Mature Trait in Kiwifruit (*Actinidia eriantha*). *Front. Plant Sci.* **2021**, *12*, 2558. [[CrossRef](#)] [[PubMed](#)]
54. Gong, C.S.; Diao, W.N.; Zhu, H.J.; Umer, M.J.; Zhao, S.J.; He, N.; Lu, X.Q.; Yuan, P.L.; Anees, M.; Yang, D.D.; et al. Metabolome and Transcriptome Integration Reveals Insights Into Flavor Formation of “Crimson” Watermelon Flesh During Fruit Development. *Front. Plant Sci.* **2021**, *12*, 629361. [[CrossRef](#)] [[PubMed](#)]
55. Li, Y.; Wang, W.; Feng, Y.; Tu, M.; Wittich, P.E.; Bate, N.J.; Messing, J. Transcriptome and metabolome reveal distinct carbon allocation patterns during internode sugar accumulation in different sorghum genotypes. *Plant Biotechnol. J.* **2019**, *17*, 472–487. [[CrossRef](#)] [[PubMed](#)]
56. Dai, Z.W.; Leon, C.; Feil, R.; Lunn, J.E.; Delrot, S.; Gomes, E. Metabolic profiling reveals coordinated switches in primary carbohydrate metabolism in grape berry (*Vitis vinifera* L.), a non-climacteric fleshy fruit. *J. Exp. Bot.* **2013**, *64*, 1345–1355. [[CrossRef](#)] [[PubMed](#)]
57. Bagri, J.; Yadav, A.; Anwar, K.; Dkhar, J.; Singla-Pareek, S.L.; Pareek, A. Metabolic shift in sugars and amino acids regulates sprouting in Saffron corm. *Sci. Rep.* **2017**, *7*, 11904. [[CrossRef](#)]
58. Song, Q.X.; Li, Q.T.; Liu, Y.F.; Zhang, F.X.; Ma, B.; Zhang, W.K.; Man, W.Q.; Du, W.G.; Wang, G.D.; Chen, S.Y.; et al. Soybean *GmbZIP123* gene enhances lipid content in the seeds of transgenic Arabidopsis plants. *J. Exp. Bot.* **2013**, *64*, 4329–4341. [[CrossRef](#)]
59. Wei, W.; Cheng, M.N.; Ba, L.J.; Zeng, R.X.; Luo, D.L.; Qin, Y.H.; Liu, Z.L.; Kuang, J.F.; Lu, W.J.; Chen, J.Y.; et al. Pitaya HpWRKY3 Is Associated with Fruit Sugar Accumulation by Transcriptionally Modulating Sucrose Metabolic Genes *HpINV2* and *HpSuSy1*. *Int. J. Mol. Sci.* **2019**, *20*, 1890. [[CrossRef](#)]
60. Peroni, F.H.G.; Koike, C.; Louro, R.P.; Purgatto, E.; do Nascimento, J.R.O.; Lajolo, F.M.; Cordenunsi, B.R. Mango starch degradation. II. The binding of α -amylase and β -amylase to the starch granule. *J. Agric. Food Chem.* **2008**, *56*, 7416–7421. [[CrossRef](#)]
61. Chou, H.L.; Dai, Z.Y.; Hsieh, C.W.; Ku, M.S.B. High level expression of *Acidothormus cellulolyticus* β -1, 4-endoglucanase in transgenic rice enhances the hydrolysis of its straw by cultured cow gastric fluid. *Biotechnol. Biofuels Bioprod.* **2011**, *4*, 1. [[CrossRef](#)]
62. Lee, H.L.; Chang, C.K.; Teng, K.H.; Liang, P.H. Construction and characterization of different fusion proteins between cellulases and β -glucosidase to improve glucose production and thermostability. *Bioresour. Technol.* **2011**, *102*, 3973–3976. [[CrossRef](#)] [[PubMed](#)]
63. Qu, Z.; Jia, Y.; Duan, Y.; Chen, H.; Wang, X.; Zheng, H.; Liu, H.; Wang, J.; Zou, D.; Zhao, H. Integrated Isoform Sequencing and Dynamic Transcriptome Analysis Reveals Diverse Transcripts Responsible for Low Temperature Stress at Anther Meiosis Stage in Rice. *Front. Plant Sci.* **2021**, *12*, 795834. [[CrossRef](#)] [[PubMed](#)]
64. Luo, X.; Wang, B.; Gao, S.; Zhang, F.; Terzaghi, W.; Dai, M. Genome-wide association study dissects the genetic bases of salt tolerance in maize seedlings. *J. Integr. Plant Biol.* **2019**, *61*, 658–674. [[CrossRef](#)]
65. Park, M.-Y.; Chung, M.-S.; Koh, H.-S.; Lee, D.J.; Ahn, S.-J.; Kim, C.S. Isolation and functional characterization of the *Arabidopsis* salt-tolerance 32 (*ATSAT32*) gene associated with salt tolerance and ABA signaling. *Physiol. Plant.* **2009**, *135*, 426–435. [[CrossRef](#)]
66. Bevilacqua, A.; Bizzarri, M. Inositols in Insulin Signaling and Glucose Metabolism. *Int. J. Endocrinol.* **2018**, *2018*, 1968450. [[CrossRef](#)]
67. Hegeman, C.E.; Good, L.L.; Grabau, E.A. Expression of D-myo-Inositol-3-Phosphate Synthase in Soybean. Implications for Phytic Acid Biosynthesis. *Plant Physiol.* **2001**, *125*, 1941–1948. [[CrossRef](#)]
68. Yang, L.; Hu, G.; Li, N.; Habib, S.; Huang, W.; Li, Z. Functional Characterization of SISAHH2 in Tomato Fruit Ripening. *Front. Plant Science.* **2017**, *8*, 1312. [[CrossRef](#)]

69. Morales, J.; Bermejo, A.; Navarro, P.; Forner-Giner, M.Á.; Salvador, A. Rootstock effect on fruit quality, anthocyanins, sugars, hydroxycinnamic acids and flavanones content during the harvest of blood oranges 'Moro' and 'Tarocco Rosso' grown in Spain. *Food Chemistry* **2021**, *342*, 128305. [[CrossRef](#)]
70. Yang, B.; He, S.; Liu, Y.; Liu, B.; Ju, Y.; Kang, D.; Sun, X.; Fang, Y. Transcriptomics integrated with metabolomics reveals the effect of regulated deficit irrigation on anthocyanin biosynthesis in Cabernet Sauvignon grape berries. *Food Chem.* **2020**, *314*, 126170. [[CrossRef](#)]
71. Tsukaya, H.; Ohshima, T.; Naito, S.; Chino, M.; Komeda, Y. Sugar-Dependent Expression of the *CHS-A* Gene for Chalcone Synthase from Petunia in Transgenic *Arabidopsis*. *Plant Physiol.* **1991**, *97*, 1414–1421. [[CrossRef](#)] [[PubMed](#)]
72. Teng, S.; Keurentjes, J.; Bentsink, L.; Koornneef, M.; Smeeckens, S. Sucrose-Specific Induction of Anthocyanin Biosynthesis in *Arabidopsis* Requires the MYB75/PAP1 Gene. *Plant Physiol.* **2005**, *139*, 1840–1852. [[CrossRef](#)] [[PubMed](#)]
73. Laurentin, A.; Edwards, C.A. A microtiter modification of the anthrone-sulfuric acid colorimetric assay for glucose-based carbohydrates. *Anal. Biochem.* **2003**, *315*, 143–145. [[CrossRef](#)] [[PubMed](#)]
74. Bolger, A.M.; Lohse, M.; Usadel, B. Trimmomatic: A flexible trimmer for Illumina sequence data. *Bioinformatics* **2014**, *30*, 2114–2120. [[CrossRef](#)] [[PubMed](#)]
75. Kim, D.; Paggi, J.M.; Park, C.; Bennett, C.; Salzberg, S.L. Graph-based genome alignment and genotyping with HISAT2 and HISAT-genotype. *Nat. Biotechnol.* **2019**, *37*, 907–915. [[CrossRef](#)] [[PubMed](#)]
76. Ghosh, S.; Chan, C.K.K. Analysis of RNA-Seq Data Using TopHat and Cufflinks. In *Plant Bioinformatics: Methods in Molecular Biology*; Springer: Cham, Switzerland, 2016; Volume 1374, pp. 339–361. ISBN 978-1-4939-3167-5.
77. Livak, K.J.; Schmittgen, T.D. Analysis of relative gene expression data using real-time quantitative PCR and the $2^{-\Delta\Delta CT}$ method. *Methods* **2001**, *25*, 402–408. [[CrossRef](#)] [[PubMed](#)]

Disclaimer/Publisher's Note: The statements, opinions and data contained in all publications are solely those of the individual author(s) and contributor(s) and not of MDPI and/or the editor(s). MDPI and/or the editor(s) disclaim responsibility for any injury to people or property resulting from any ideas, methods, instructions or products referred to in the content.